TOPOLOGICAL INSULATOR HETEROSTRUCTURES

by

Mahmoud Lababidi
A Dissertation
Submitted to the
Graduate Faculty
of
George Mason University
in Partial Fulfillment of
The Requirements for the Degree
of
Doctor of Philosophy
Physics

Committee:

_____ Dr. Erhai Zhao,
Dissertation Director

_____ Dr. Dimitrios A. Papaconstantopoulos,
Committee Member

_____ Dr. Predrag Nikolic,
Committee Member

_____ Dr. Qiliang Li,
Committee Member

_____ Dr. Michael E. Summers,
Department Chair

_____ Dr. Timothy L. Born,
Associate Dean for Student and Academic
Affairs, College of Science

_____ Dr. Vikas Chandhoke, Dean,
College of Science

Date: _____ Summer Semester 2013
George Mason University
Fairfax, VA

Topological Insulator Heterostructures

A dissertation submitted in partial fulfillment of the requirements for the degree of Doctor of Philosophy at George Mason University

By

Mahmoud Lababidi
Bachelor of Science
University of Florida, 2006

Director: Dr. Erhai Zhao, Professor
School of School of Physics, Astronomy and Computational Science

Summer Semester 2013
George Mason University
Fairfax, VA

Dedication

To Angus Macgyver, who needed only a roll of duct tape,
paperclip, and a Swiss Army knife to solve any problem.
To my parents, Lina and Steve, for committing their lives
for me, my future, and my success and happiness in life.

Acknowledgments

First and foremost, I'd like to thank the most impressionable, understanding and supportive advisor anyone could ask for, Erhai Zhao. Not only have I learned more about physics than I could ever imagine, he has mentored me on being a good scientist, and a disciplined worker. I really could not have asked for a better advisor to lead me through this fascinating journey. I'd like to thank Dr. Papa for his incredible generosity from day one. He supported me throughout my PhD and without that support I would not have succesfully completed the many projects and publications I have had. I consider Paul So to be more than just a graduate department advisor. You could add resident psychologist to his title and it would be wholly appropriate. Without his clear guidance on all topics, including ones beyond physics and art, I would be a lost soul. I thank Mike Summers for his help as a department chair and helping me in times in need. He's supported me financially at times and has always had an open door for me and any graduate student to talk to him. Joe Weingartner would be considered the "House Dad" of the fraternity of the physics department. He has been a guiding light to me in many ways including physics and life. He is without a doubt one of the most important people the department has given tenure to for his kindness and empathy for anyone who walks into his office. I am very grateful to Indu Satija for her amazing creativity and beautiful ability to see physics like no one has. I give her full credit for the idea that spawned my most fascinating project of the driven quantum Hall system. I thank Predrag Nikolic, not only as helpful committee member but as great educator. He has always welcomed healthy discussion about a variety of topics that have helped me in my career numerous times. Qilian Li has been one of the most excited and appreciative members I could have on my committee. His enthusiasm in my work has been a heavy driver for a signifact portion of my research. Ming Tian was the first person to take me in under her wing as a student. She saw I had potential and ability to do physics and immediately gave me challenging problems to work on. She has been very supportive of my endeavours even if it meant changing groups. Without Kathleen Enos, Mari-Elaine Triolo, Geoff Elkins, Stephanie Monk, and Melissa Hayes I would be wrapped up in more paperwork than I could handle. They have made my this trip as smooth as possible and have been the best people to have around. Of course without Dan Thomas and Andrew Abdalian I'd be a headless chicken running around with regards to my IT issues. Phil Rubin was the person that urged me to apply to the program regardless of my physics background because he believed I'd do great. Somehow he was right. I later learned Phil was in a psychology PhD program when he switched to physics. That's serious inspiration. Gerald Cook was the first Professor I interacted with in my desire to start back in grad school. He was very enthusiastic for me to begin this journey. Stephen Gildea for inspiring me to go to graduate school by becoming a rocket scientist and kicking ass at it. Anish Mitra, my first friend in graduate school and roommate deserves much recognition for being the one person that was as interested in math and science as I was. Indrajit Das and Zrinka Greguric Ferencek are staples in my early career. I owe much to them for their stimulating discussions while we completed

course work together. Timofey Frolov is my favorite Russian physicist, metal guitarist, food snob I've ever known. He has been a great friend and colleague during our years at GMU before he ditched me for Berkeley. Ol' Dirty himself, Greg Byrne, deserves more than a mention here for our antics during these years especially at the Arlington Office. Many thanks go to Devin Vega and our enjoyable and stimulating discussions in course work and research under Ming Tian. Quite importantly, I'd like to thank Lois Cohen, Edmund Lau, and Jean Wright for their influence during my formative high school years. I owe them more than just a line in this theses and without them I truly would not be here. The same goes for Anand Rangarajan and Eric Schwartz from my time at University of Florida, two professors who challenged me in innovative and creative ways. Not least, I'd like to thank SPACS, Office of Naval Research and National Institute of Standards and Technology for the funding they have provided me over these years.

Table of Contents

List of Figures

List of Symbols

v_F	Fermi velocity of Dirac electrons
$\vec{k}$	momentum vector
k_i	momentum in the i-th direction
$\mathcal{E}_F$	Fermi energy
$A(x, k, \epsilon)$	spin(σ), momentum and position resolved density of (energy) states
$N(x, \epsilon)$	spin(σ) and position resolved density of (energy) states
μ	chemical potenial, sometimes as Fermi energy ($\mathcal{E}_F$)
$\mathcal{H}$	Hamiltonian
$\psi(x)$	wave function of particle
u_σ (v_σ)	Bogoliubov-de Gennes quasi-particle (hole) wave function
k_B	Boltzmann's constant

Abstract

TOPOLOGICAL INSULATOR HETEROSTRUCTURES

Mahmoud Lababidi, PhD

George Mason University, 2013

Dissertation Director: Dr. Erhai Zhao

Abstract here.

Chapter 1: Introduction

This thesis is broken down into five chapters that represent the work in the studies of topological insulators (TI) and superconductors along with additional appendices related to topological materials. Beyond the first introductory chapter on topological insulators, superconductors and their interaction together, the chapters are divided out categorically with increasing level of depth and complexity in the study of superconductivity. The second chapter presents a study of metal on TI (M-TI) scattering and interaction, which provides intuition to understanding the effect of spin-orbit interactions to arbitrary spin-polarized electrons. The second chapter begins the process of the study of superconductors with topological insulators, where an exploration of the cooper pairing, the primary mechanism behind superconductivity, and its penetration into a TI as well as the reverse effect of spin-orbit effects into a superconductor. The third chapter takes the resulting superconducting proximity induced surface state on a TI surface and delves into the Josesphon junction, and in particular the π state. The fourth chapter describes an investigation on the newly proposed scheme to engineer a gapless Weyl superconductor through layering of superconductors and TI. Each of the chapters has an introduction section that outlines how the focused study plays a role in the larger scheme of the thesis. It will also give an overview of the chapter and what parts have been published.

1.1 Topological Insulators

The field of condensed matter physics has a history of understanding phases of matter that have been condensed where the early focus was on solids and liquids. The field has transitioned into studying a variety of novel phases that are very rich and complex in physical phenomena. A result of the exploration of many novel phases, the concept of order

arose, allowing, not only the ability to categorize these phases by recognizing the type of order the system had but the order and symmetry actually described the physical system and allowed a deeper understanding. This idea is clearly seen in the phase transition of liquid atoms with rotational and translational symmetry into a crystal with discrete symmetries (e.g. translational, discrete rotational, inversion). An extension to this would be a solid transitioning into a magnet, thus breaking inversion symmetry. While this study of symmetry breaking is at the heart of condensed matter, it is not the full story.

In 1980 Klaus von Klitzing performed an experiment measuring the Hall conductance of a special semiconductor heterostructure. What he found in the experiment was that the measured conductance came in exact quantized fundamental units of

$$\sigma = \nu \frac{e^2}{h}, \tag{1.1}$$

where ν is an integer value. The significance of this result, was not only in the quantized nature of the Hall conductance, but something a bit deeper. This quantum Hall effect was special because in this result could not be predicted through the usual symmetry breaking language. In the heterostructure used in the experiment, the internal "bulk" of the system is effectively a two dimensional electron gas exposed to a strong magnetic field. The strong magnetic field puts the electrons in a cyclotron orbit and forces the electrons into discrete energy levels, Landau levels. This effect is the same as a harmonic oscillator where an electron is in a spatially quadratic electric potential well ($V(x) \propto x^2$). These separated energy levels allows for the system to be an insulator when the Fermi energy is placed within the gap between to energy levels. While this system is in an insulating state, the special result of von Klitzing's experiment is that the edge is still a host to electronic states. These edge electrons also propagate in a restricted chiral manner. This discrepancy between the ability to describe bulk of the material and its edge is the issue at hand.

The quantum Hall effect (QHE) is actually a topological phase, meaning it has topological order. Systems with topological order have long-range entanglement and a ground state

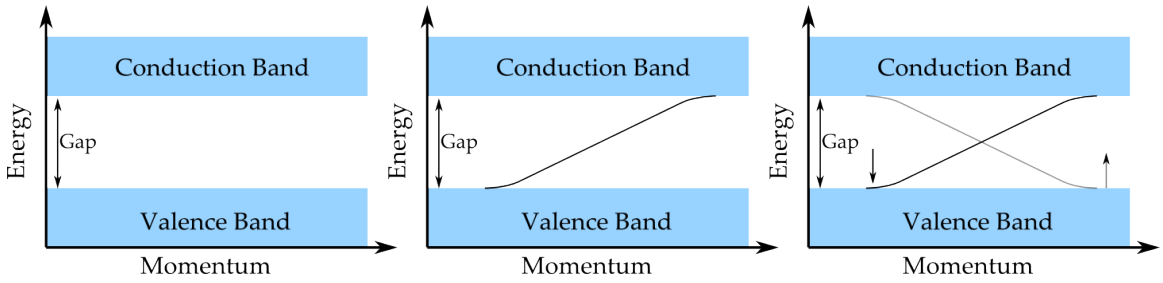

Figure 1.1: (a) Energy spectrum of a trivial band insulator where two bands, conduction and valence are separated by an energy gap. (b) Energy spectrum of a quantum hall state. The gap now has one chiral edge state connecting the valence band to the conduction band. (c) Energy spectrum of a 2D TI (QSH). The gap now has one pair of chiral edge states connecting the valence band to the conduction band. One line is for the spin up state and the other is for the spin down state. This essentially mimics two copies of the quantum hall state for each spin.

degeneracy that cannot be lifted by any local perturbation. These systems are protected from being deformed into a phase with different topology in the same way a donut (torus) is protected from being deformed into a sphere. The only time such a change is possible is through a phase transition where the gap in the energy spectrum closes in a critical fashion. Many discussions on topological order can be found in many literature and any continued discussion about topological order in farther depth would not be appropriate, for this thesis does not represent any study of topological order in this form.

We, instead, will continue by using the QHE as a lead-in for the topological insulator. Though the topological insulator is a slight misnomer because of the lack of topological order (i.e. long-range entanglement), we will shortly see where the topology plays a role in it. By taking the QHE, we can extend it in the following way. The QHE is a gapped system with chiral edge states that depend on the applied magnetic field (see Fig. The chirality of the edge states depend on the direction of the magnetic field, i.e. positive (negative) chiral motion of the electrons for positive (negative) in-plane magnetic field. If a system were to have both positive and negative magnetic fields simultaneously for two different species of electrons, we would see the electrons follow the two chiral motions simultaneously depending on their species. The two different species of electrons are, of course, spin-up and spin-down electrons which couple to the two magnetic fields. This system is the quantum spin hall

effect. This system, first introduced by Kane and Mele, was proposed to exist in graphene. Shortly afterwards Bernevig, Hughes, and Zhang proposed an experimental setup to host the QSH effect. Their proposal, which was verified successfully in an experiment by Koenig, exploited the spin-orbit coupling and band inversion in a HgTe CdTe HgTe heterostructure, which allowed for simultaneous opposite chirality edge states. The QSH insulator, is a 2D topological insulator. An effective Hamiltonian for the edge state can be written as

$$H = \hbar v_F \sigma_x k_y, \tag{1.2}$$

where the basis is for spin up and spin down and the resulting eigen energies are $E = \pm\hbar v_F k_y$. $\hbar v_F$ is the Fermi velocity slope. This is a massless Dirac Hamiltonian and the spectrum forms a Dirac crossing.

In principle, by stacking sheets of the 2D TIs and forming a 3D structure, this would be a "weak" topological insulator. The other extension of the TI from 2D to 3D would be to have an insulating 3D bulk and the surfaces interfacing the vacuum. These surface states are similar to the 2D edge state in their linear dispersing behavior, but in contrast they can have momentum in any direction, $\vec{k} = (k\cos(\theta), k\sin(\theta))$. The effective low-energy Hamiltonian for these surface states,

$$H = \hbar v_F(\sigma_x k_y - \sigma_y k_x), \tag{1.3}$$

and the energies, $E = \pm\hbar v_F|\vec{k}|$, where $|\vec{k}| = \sqrt{k_x^2 + k_y^2}$. This is a "strong" topological insulator. When varying a parameter of an insulator to transition it from topological to trivial the bulk gap must close. The surface state is exactly that because the vacuum is a trivial insulator. Any surface on the TI that interfaces with the vacuum has a closed gap and is host to the Dirac fermion surface states.

A simple exercise to see the insulator-surface state behavior described, we present a

simplified version of the accepted model Hamiltonian for bulk Bi_2Se_3:

$$H = (M_0 + Mk^2)\tau_z + A(\sigma_x k_y - \sigma_y k_x)\tau_x + B\sigma_z k_z \tau_y, \tag{1.4}$$

where $\sigma(\tau)$ represent spin (orbital) basis, $A, B, M, M0$ represent physical parameters of the system. This Hamiltonian can be diagonalized to find energy eigenvalues of

$$E = \pm\sqrt{(M_0 + Mk^2)^2 + A^2(k_x^2 + k_y^2) + B^2 k_z^2}. \tag{1.5}$$

A three step inspection can show how two critical ingredients are needed for this to be a topological insulator. By setting $A = B = 0$ and having $M_0 > 0$, we see that we have a trivial insulator with a band-gap of $2M_0$. By adjusting this gap parameter to negative values, $M_0 < 0$, we see the valence and conduction bands intersect at $E = 0$. To transition this to an insulator we can set $A \neq 0$ and $B \neq 0$, in effect turning on spin orbit coupling. We now see a gap arise and through additional steps we find that this setup is host to surface states. To find these surface states we set the form of the wave functions to be

$$\psi \propto e^{\Lambda z} \tag{1.6}$$

as an ansatz from an assumption that $H(x, y, z = 0, L) = 0$ and that the surface states reside on the boundaries decay into the bulk. We also make the substitution of $k_z \to -i\partial_z$. The Hamiltonian is now in the form

$$H = (M_0 + M(k_x^2 + k_x^2 - \Lambda^2))\tau_z + A(\sigma_x k_y - \sigma_y k_x)\tau_x + B\sigma_z(-i)\Lambda\tau_y. \tag{1.7}$$

To verify the existence of a Dirac crossing at zero energy, we diagonalize the Hamiltonian and set $k_x = k_y = E = 0$ and find that there exists values for Λ:

$$\Lambda = \pm\frac{B \pm \sqrt{B^2 + 4MM_0}}{2M} \tag{1.8}$$

illustrating that surface states do indeed exist.

This concludes the basic description of the TI. We showed how a 2D TI was produced using two copies of a QH system with opposite simultaneous magnetic fields. We then extended the idea of a 2D TI to 3D "weak" and "strong" TIs. We then took the bulk system and used it to find an existence surface states. and we proceed into a discussion of superconducting phases of matter.

1.2 Superconductivity

1.2.1 Measurement

The discovery of superconductivity by Heike Kamerlingh Onnes is usually the first item that's discussed when the topic of superconductivity is brought up. In the discovery, Onnes found that the resistance of mercury drops to zero, a signature of perfect conduction. The immediate question that rang in my head, if using a typical voltmeter, as used in physics labs, and Ohm's law, $V = IR$, how can resistance or voltage be measured if they should both be zero? The result is by using a four point probe. As seen in the diagram in Fig. 1.2, the probe has four point of contact on the material. Two of the connections (1,4) have a constant, controllable current flowing through them. The other two connections (2,3), then probe the sample and measure the voltage drop. The voltage measurement device has a high impedance to minimize any flow from the sample to flow into it. The resulting voltage drop, V, and driving current, I, then give the resistance, $R = V/I$, which along with temperature results in a temperature dependent resistance. An example measurement of $Cu_{.2}Bi_2Se_3$, a new superconducting material is shown in Fig. 1.2. The plot shows a clear resistance drop at 3.5 Kelvin, the signature of superconductivity.

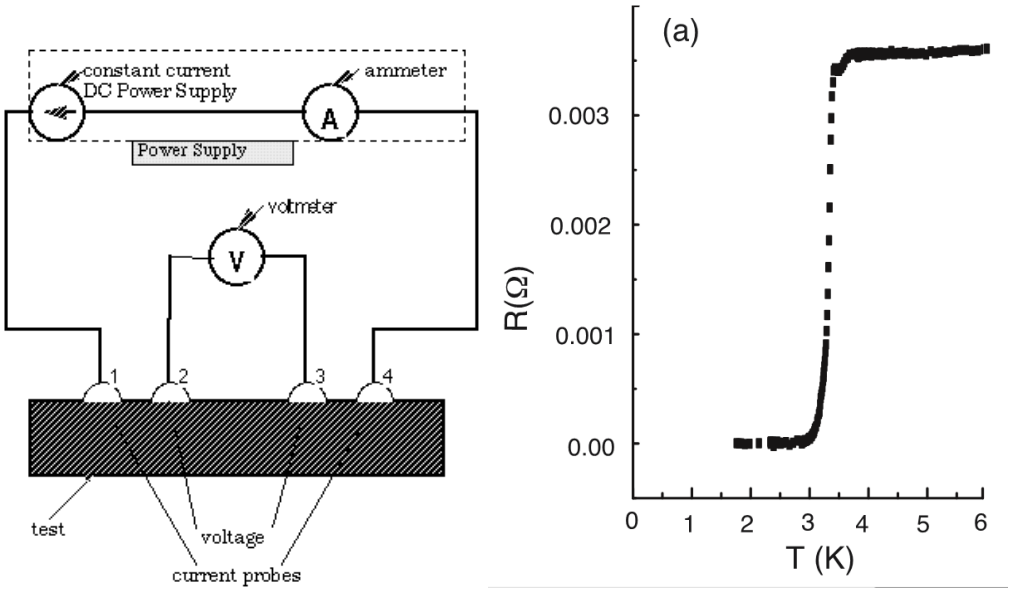

Figure 1.2: (left) Four probe measurement device. Probes 1 and 4 are used to flow a current across a sample while probes 2 and 3 measure the voltage drop across the sample where the current is flowing. (right) Resistance (Ω) vs Temperature (Kelvin) experiment on $Cu_{.2}Bi_2Se_3$ from arXiv:1111.5805. The drop in resistance is a signature of superconductivity.

1.2.2 BCS and Bogoliubov Theory

Now that the question of how to find and measure superconductivity is out of the way, we can look at the theory that Bardeen, Cooper, and Schreiffer (BCS) came up to explain the mechanism behind superconductivity. We start with the Hamiltonian that represents a free electron system with two-body electron interactions,

$$H = \sum_{\mathbf{k},\sigma} (\epsilon_{\mathbf{k}} - \epsilon_F) c^\dagger_{\mathbf{k}\sigma} c_{\mathbf{k}\sigma} + \sum_{\mathbf{k},\mathbf{l}} V_{\mathbf{kl}}\, c^\dagger_{\mathbf{k}\uparrow} c^\dagger_{-\mathbf{k}\downarrow} c_{-\mathbf{l}\uparrow} c_{\mathbf{l}\downarrow} \tag{1.9}$$

where $c^\dagger_{\mathbf{k}\sigma}$ ($c_{\mathbf{k}\sigma}$) is the electron creation (annhialation) operator, the summations are over spin (σ)and momentum ($\mathbf{k}, \mathbf{l}$), $\epsilon_{\mathbf{k}}$ is the free electron energy, $V_{\mathbf{kl}}$ is the electron-electron interaction potential. The commutation relations for the fermionic creation and annihilation operators are

$$\{c^\dagger_{\mathbf{k}\sigma}, c_{\mathbf{k}'\sigma'}\}_+ = \delta(\mathbf{k} - \mathbf{k}')\delta_{\sigma\sigma'} \tag{1.10}$$

$$\{c^\dagger_{\mathbf{k}\sigma}, c^\dagger_{\mathbf{k}'\sigma'}\}_+ = \{c_{\mathbf{k}\sigma}, c_{\mathbf{k}'\sigma'}\}_+ = 0. \tag{1.11}$$

In usual electron systems, the interaction scattering potential, $V_{\mathbf{kk}'}$, usually positive, represents repulsive interactions. But as the temperature is lowered, what BCS explained was that the repulsive interaction was no longer the dominant interaction. Instead, what occurs at zero temperature is the following. As an electron passes through a lattice of low-mobility nuclei, they actually cause the nuclei to shift causing a phonon interaction with electron. This phonon interaction is enough to effectively attract, $V_{\mathbf{kk}'} < 0$, two electrons with opposite momenta$(\mathbf{k}, -\mathbf{k})$. From the Pauli exlusion principle, we seek a bound pair of electrons with zero momentum, antisymmetric, spinless properties, known as a Cooper pair. This pair of electrons forms a boson with superflow that is responsible for the lack of resistance. The electrons near the Fermi energy are most succeptible to pairing, usually when they are within some Debye energy cutoff, $\hbar\omega_D$. When the electrons pair, they form a condensate of the bosons. One way to describe these bosons is through a condensate

wave function, $\Delta(\mathbf{x})$, or $\Delta_{\mathbf{k}}$. This function is found by a mean field approach to the pairing potential, $V_{\mathbf{k}\mathbf{k}'}$, through the gap equation

$$\Delta_{\mathbf{k}} = \sum_{\mathbf{k}'} c_{-\mathbf{l}\uparrow} c_{\mathbf{l}\downarrow} \tag{1.12}$$

reducing the Hamiltonian down to

$$H = \sum_{\mathbf{k},\sigma} (\epsilon_{\mathbf{k}} - \epsilon_F) c^\dagger_{\mathbf{k}\sigma} c_{\mathbf{k}\sigma} + \sum_{\mathbf{k}} \Delta_{\mathbf{k}}\, c^\dagger_{\mathbf{k}\uparrow} c^\dagger_{-\mathbf{k}\downarrow}. \tag{1.13}$$

To diagonalize this hamiltonian we change the basis, where rather than restricing ourselves to operators of electrons, we use the Bogoliubov-deGennes (BdG) transformation to convert the operators on elementary quasiparticle excitations of particles and holes. This is done through

$$c_{\mathbf{k}\sigma} = \sum_n u_{n\mathbf{k}\sigma} \gamma_{n\mathbf{k}} + v^*_{n\mathbf{k}\sigma} \gamma^\dagger_{n\mathbf{k}}, \quad c^\dagger_{\mathbf{k}\sigma} = \sum_n u^*_{n\mathbf{k}\sigma} \gamma^\dagger_{n\mathbf{k}} + v_{n\mathbf{k}\sigma} \gamma_{n\mathbf{k}} \tag{1.14}$$

where the BdG operators fulfill the anticommutation relations,

$$\{\gamma^\dagger_{\mathbf{k}\sigma}, \gamma_{\mathbf{k}'\sigma'}\} = \delta_{\mathbf{k}\mathbf{k}'}\delta_{\sigma\sigma'} \qquad \{\gamma_{\mathbf{k}\sigma}, \gamma_{\mathbf{k}'\sigma'}\} = \{\gamma^\dagger_{\mathbf{k}\sigma}, \gamma^\dagger_{\mathbf{k}'\sigma'}\} = 0 \tag{1.15}$$

and allow us to diagonalize the Hamiltonian as

$$H = E_0 + \sum_{\mathbf{k},\sigma} E_{\mathbf{k}} \gamma^\dagger_{\mathbf{k}\sigma} \gamma_{\mathbf{k}\sigma}. \tag{1.16}$$

The quasiparticle (quasihole) wave function is $u_{\mathbf{k}\sigma}$ ($v_{\mathbf{k}\sigma}$). Each electron creation/annihilation operator is a superposition of a quasiparticle creation and annihilation operator. The inverse

of this transformation,

$$\gamma_{\mathbf{k}\sigma} = \sum_n u_{n\mathbf{k}\sigma} c_{n\mathbf{k}} - v^*_{n\mathbf{k}\sigma} c^\dagger_{n\mathbf{k}}, \quad \gamma^\dagger_{\mathbf{k}\sigma} = \sum_n u^*_{n\mathbf{k}\sigma} c^\dagger_{n\mathbf{k}} - v_{n\mathbf{k}\sigma} c_{n\mathbf{k}} \tag{1.17}$$

leads to each quasiparticle operator being a superposition of one electron creation operator and one hole creation operator, thus the sum net charge is zero for each BdG creation/annihilation operator. This physical interpretation allow us to see that there is more to the story than just electrons and holes, but elementary quasiparticle excitations of pairs of holes and electrons.

The form of the BdG Hamiltonian is

$$H_B = \begin{pmatrix} \epsilon_{\mathbf{k}} - \epsilon_F & -\Delta_{\mathbf{k}}\, i\sigma_y \\ \Delta^*_{\mathbf{k}}\, i\sigma_y & \epsilon_F - \epsilon_{\mathbf{k}} \end{pmatrix}, \tag{1.18}$$

in the basis of

$$\psi = \left(u_{\mathbf{k}\uparrow}, u_{\mathbf{k}\downarrow}, v_{\mathbf{k}\uparrow}, v_{\mathbf{k}\downarrow}\right)^T. \tag{1.19}$$

The $\Delta_{\mathbf{k}}$ can come in a variety of forms, strictly depending on the pairing symmetry of the superconductor. In the BCS case, we focus on $\Delta_{\mathbf{k}} = \Delta_0$, a constant value, representing s-wave orbital pairing. This allows us to find the eigen values of the system,

$$E_{\mathbf{k}} = \pm\sqrt{(\epsilon_{\mathbf{k}} - \epsilon_F)^2 + |\Delta|^2}. \tag{1.20}$$

where the spectrum can be seen in the Fig. 1.3. There is now a finite gap of size $2\Delta_0$ seen centered about 0. The gap is a result of the pairing that occurs in the superconductor. These paired states form the condensate, Δ, and no low energy excitations can exist within the energy gap in the spectrum. In order for an excitation to move a paired state out of the condensate, you would need Δ_0 energy to break the pair.

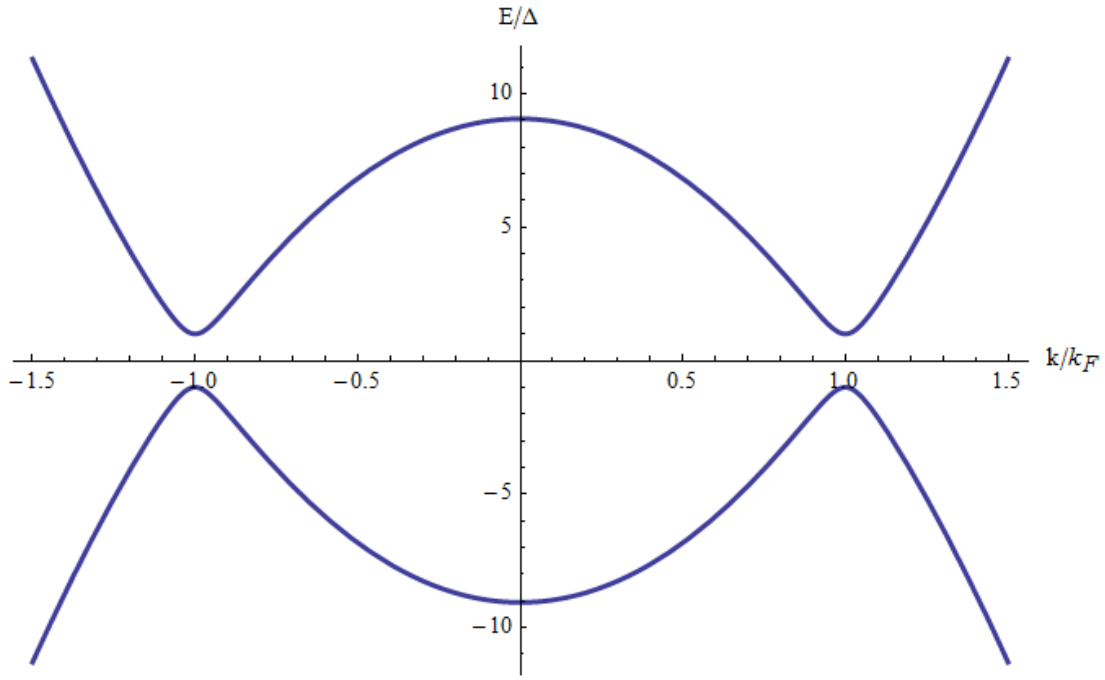

Figure 1.3: Energy spectrum for a BCS superconductor with a gap of $2\Delta_0$ and $\epsilon_F/\Delta_0 = 10$.

This concludes the section on superconductivity. Here we described a basic idea on how to measure a superconductor using a four-probe measurement, we describe the BCS theory on superconductivity to describe the mechanism behind the Cooper pairing, and we diagonalized the BCS Hamiltonian using a mean field approximation and a Bogoliubov-de Gennes Transformation, which allowed us to investigate the energy spectrum. These should be the building blocks for understanding the discussion on superconductivity in this thesis.

Chapter 2: Metal to Topological Insulator Scattering

We compute the spin-active scattering matrix and the local spectrum at the interface between a metal and a three-dimensional topological band insulator. We show that there exists a critical incident angle at which complete (100%) spin flip reflection occurs and the spin rotation angle jumps by π. We discuss the origin of this phenomena, and systematically study the dependence of spin-flip and spin-conserving scattering amplitudes on the interface transparency and metal Fermi surface parameters. The interface spectrum contains a well-defined Dirac cone in the tunneling limit, and smoothly evolves into a continuum of metal induced gap states for good contacts. We also investigate the complex band structure of Bi_2Se_3.

2.1 Introduction

Recently discovered three dimensional topological band insulators [**?**, **?**, **?**], such as $Bi_{1-x}Sb_x$ [**?**] and Bi_2Se_3 [**?**, **?**, **?**], are spin-orbit coupled crystal solids with a bulk gap but protected gapless surface states. The low energy excitations at the surface are helical Dirac fermions, i.e., their spin and momentum are entangled (locked) [**?**]. The charge and spin transport on the surface of a topological insulator are intrinsically coupled [**?**]. This makes these materials a promising new platform for spintronics. In addition, heterostructures involving topological insulator, superconductor, and/or ferromagnet have been predicted to show a remarkable array of novel spectral and transport properties (for review see Ref. [**?**, **?**, **?**]).

Electronic or spintronic devices based on topological insulators will almost inevitably involve metal as measurement probes or functioning components [**?**]. This motivates us to study the local spectrum near the interface between a metal (M) and a topological insulator (TI). For a metal-ordinary semiconductor junction with good contact, it is well known that

the metallic Bloch states penetrate into the semiconductor as evanescent waves localized at the interface (for energies within the band gap). Such interface states are known as metal induced gap states (MIGS) [**?**, **?**]. They play an important role in controlling the junction properties, e.g., by pinning the semiconductor Fermi level to determine the Schottky barrier height [**?**], a key parameter of the junction.

The local spectrum at the M-TI junction is intimately related to the spin-active scattering of electrons at the M-TI interface. In this paper, we systematically study the evolution of the scattering matrix and the interface spectra with the junction transparency and metal Fermi surface parameters. The scattering matrix [**?**] we obtain here also forms the basis to investigate the details of the superconducting proximity effect near the superconductor-TI interface [**?**], which was shown by Fu and Kane to host Majorana fermions [**?**].

The scattering at the M-TI interface differs significantly from its two dimensional analog, the interface between a metal and a quantum spin Hall (QSH) insulator studied by Tokoyama et al [**?**]. They predicted a giant spin rotation angle $\alpha \sim \pi$ and interpreted the enhancement as resonance with the one-dimensional helical edge modes. By contrast, for M-TI interface we predict a critical incident angle at which complete spin flipping occurs and the spin rotation angle jumps by π. We will explain its origin, in particular its relation to the surface helical Dirac spectrum, and discuss its spintronic implications.

This paper is organized as follows. We will first compute the scattering matrix using a $\mathbf{k} \cdot \mathbf{p}$ continuum model by matching the envelope wave functions at the M-TI interface. This simple calculation is easy to understand, and it brings out the main physics of our problem. Along the way, we will discuss the complex band structure of Bi_2Se_3, which describes the decaying (rather than propagating Bloch wave) solutions of the crystal Hamiltonian. The various caveats of this calculation are then remedied by considering a much more general lattice model. Most importantly, it enables us to track how the scattering matrix and interface spectrum change with interface transparency. It also sheds light on the origin of perfect spin-flip scattering at the critical angle. We will show that the results obtained from these two complementary methods are consistent with each.

2.2 Model Hamiltonian and Complex Band Structure

We consider Bi_2Se_3 as a prime example of 3D strong topological insulators. Its low energy $\mathbf{k}\cdot\mathbf{p}$ Hamiltonian was obtained by Zhang et al [**?**],

$$\hat{H}_{TI}(\mathbf{k}) = \epsilon_0(\mathbf{k})\hat{1} + \sum_{\mu=0}^{3} d_\mu(\mathbf{k})\hat{\Gamma}_\mu.$$

Here $d_0(\mathbf{k}) = M - B_1k_z^2 - B_2(k_x^2+k_y^2)$, $d_1(\mathbf{k}) = A_2k_x$, $d_2(\mathbf{k}) = A_2k_y$, $d_3(\mathbf{k}) = A_1k_z$, and $\epsilon_0(\mathbf{k}) = C + D_1k_z^2 + D_2(k_x^2+k_y^2)$. The numerical values of M, A, B, C, D are given in Ref. [**?**]. We choose the basis ($|+\uparrow\rangle$, $|+\downarrow\rangle$, $|-\uparrow\rangle$,$|-\downarrow\rangle$), where $\pm$ labels the hybridized p_z orbital with even (odd) parity [**?**]. The Gamma matrices are defined as $\hat{\Gamma}_0 = \hat{\tau}_3\otimes\hat{1}$, $\hat{\Gamma}_i = \hat{\tau}_1\otimes\hat{\sigma}_i$, with $\hat{\tau}_i$ ($\hat{\sigma}_i$) being the Pauli matrices in the orbital (spin) space. The chemical potential of as-grown Bi_2Se_3 crystal actually lies in the conduction band [**?**]. By hole doping [**?**] or applying a gate voltage [**?**], the chemical potential can be tuned inside the gap. The system is well described by H_{TI} (note that energy zero is set as in the middle of the band gap).

In this section, we first adopt a rather artificial model for metals with negligible spin-orbit coupling. It is obtained by turning off the spin-orbit interaction (setting $d_\mu = 0$ for μ=1,2,3) in H_{TI} and shifting the Fermi level into the conduction band. The result is spin-degenerate two-band Hamiltonian

$$\hat{H}_M(\mathbf{k}) = [\epsilon_0(\mathbf{k}) - E_F]\hat{1} + d_0(\mathbf{k})\hat{\Gamma}_0.$$

Its band structure, schematically shown in Fig. 1(b), consists of two oppositely dispersing bands (the solid and dash line). E_F is tuned to be much higher than the band crossing point, so the scattering properties of low energy electrons near the Fermi surface are insensitive to the band crossing at high energies. This claim will be verified later using a more generic model for the metal. A similar model was used in the study of metal-QSH interface [**?**].

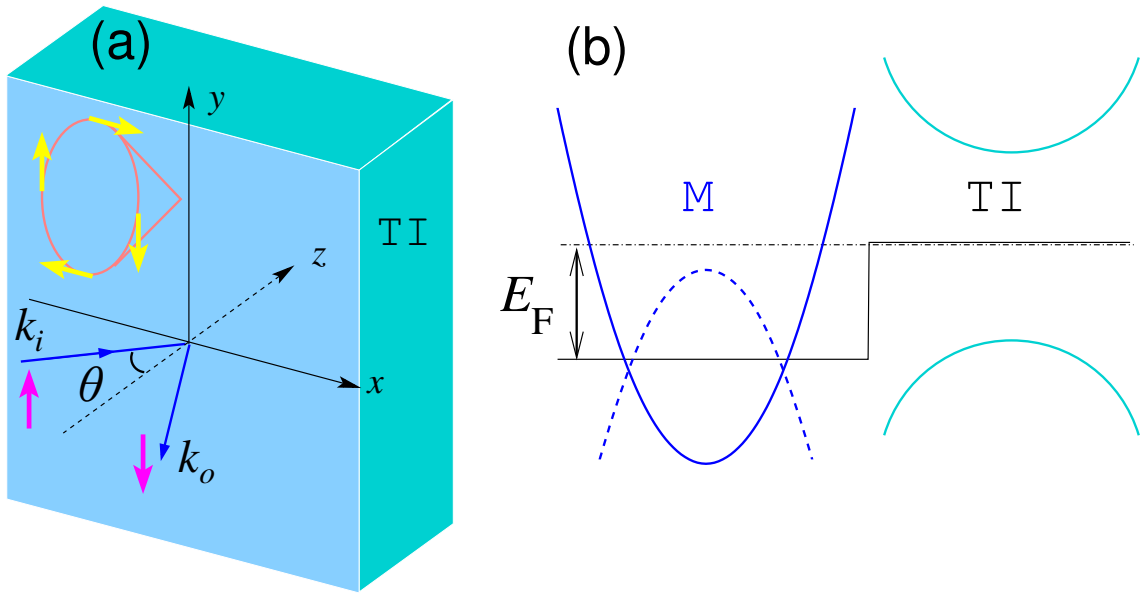

Figure 2.1: (a) Scattering geometry at a metal (M)-topological insulator (TI) interface. (b) Schematic band structure of the metal (modeled by $\hat{H}_M$) and topological insulator.

Matching the wave functions of two dissimilar materials (such as Au and Bi_2Se_3) at interface is in general complicated within the $\mathbf{k}\cdot\mathbf{p}$ formalism, because the envelope wave functions on either side are defined using different basis (see Ref. [?] and reference therein). For the particular model H_M, however, such complication is circumvented. Then, then wave functions at the metal-TI interface ($z = 0$) satisfy the Ben-Daniel and Duke boundary condition [?],

$$\hat{\Phi}_M = \hat{\Phi}_{TI}, \quad \hat{v}_M\hat{\Phi}_M = \hat{v}_{TI}\hat{\Phi}_{TI}.$$

Here $\hat{\Phi}_i$ is the four-component wave function, and the velocity matrix $\hat{v}_i = \partial\hat{H}_i/\partial k_z$, $i \in \{M, TI\}$. Such boundary condition assumes good atomic contact between two materials.

We are interested in energies below the band gap of TI, so $\hat{\Phi}_{TI}$ is evanescent in nature and only penetrates into TI for a finite length. Such localized (surface or interface) states inside topological insulator can be treated within the $\mathbf{k}\cdot\mathbf{p}$ formalism using the theory of *complex band structures*, pioneered by Kohn [?], Blount [?], and Heine [?] et al. The main idea is to allow the crystal momentum to be complex and analytically continue $H_{TI}(\mathbf{k})$ to

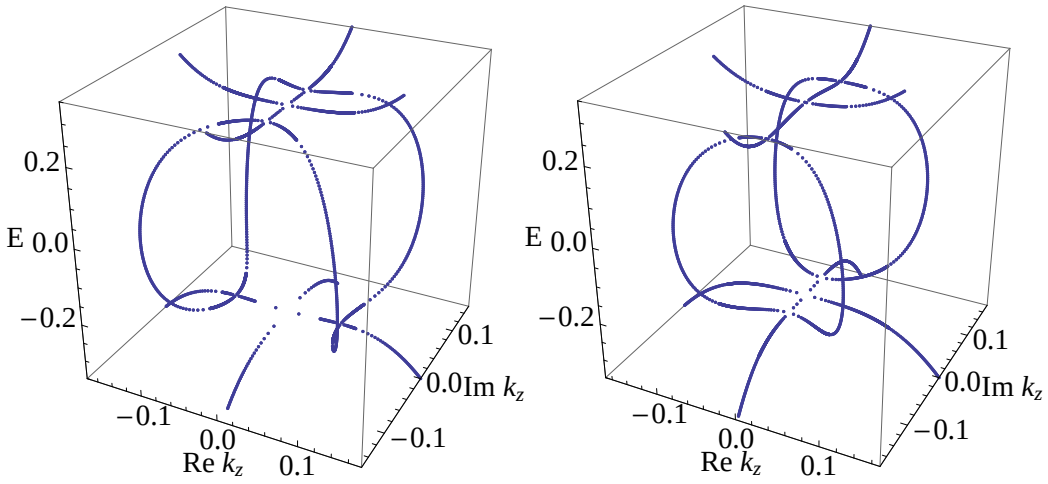

Figure 2.2: The complex band structure of topological insulator described by $\hat{H}_{TI}(\mathbf{k})$ for $k_y = 0$, $k_x = 0.02$ (left) and 0.04 (right). E is measured in eV, and k in Å^{-1}. Subgap states with complex k_z represent evanescent waves. The topology of real lines [**?**] changes as k_x is increased.

the complex $\mathbf{k}$ plane. While the extended Bloch waves are the eigen states of $H_{TI}(\mathbf{k})$ for real $\mathbf{k}$, eigen functions of $H_{TI}(\mathbf{k})$ for complex $\mathbf{k}$ describe localized states. Together they form a complete basis to describe crystals of finite dimension.

In our scattering problem, we have to find all eigen states of $H_{TI}(\mathbf{k})$ with energy E and wave vector $\mathbf{k} = (k_x, k_y, \tilde{k}_z)$, where k_x and k_y are given and real, but $\tilde{k}_z$ is complex and unknown. For a general $\mathbf{k}\cdot\mathbf{p}$ Hamiltonian such as $\hat{H}_{TI}$, we follow Chang and Schulman [**?**] to rewrite it as

$$\hat{H}_{TI} = \hat{h}_0(k_x, k_y) + \hat{h}_1\tilde{k}_z + \hat{h}_2\tilde{k}_z^2,$$

where $\hat{h}_1 = A_1\hat{\Gamma}_3$, and $\hat{h}_2 = -B_1\hat{\Gamma}_0$. Then the eigen equation $(\hat{H}_{TI} - E\hat{1})\hat{\phi} = 0$ can be reorganized into an eigen value problem for $\tilde{k}_z$,

$$\begin{pmatrix} 0 & 1 \\ -\hat{h}_2^{-1}(\hat{h}_0 - E\hat{1}) & -\hat{h}_2^{-1}\hat{h}_1 \end{pmatrix} \begin{pmatrix} \hat{\phi} \\ \hat{\phi}' \end{pmatrix} = \tilde{k}_z \begin{pmatrix} \hat{\phi} \\ \hat{\phi}' \end{pmatrix}.$$

Then all possible values of $\tilde{k}_z$ can be obtained for given incident parameter E, k_x, and

k_y. For the anisotropic Dirac Hamiltonian $H_{TI}(\mathbf{k})$, the energy eigenvalues can be obtained analytically [**?**], which allows for an analytical solution of the complex band structure.

For E within the gap, there are in general 4 pairs of complex solution of $\tilde{k}_z$, for if $\tilde{k}_z$ is a solution so is $\tilde{k}_z^*$. We label those with positive imaginary parts with $\{\tilde{k}_z^\nu\}$, and the corresponding wave function $\{\hat{\phi}^\nu\}$, $\nu = 1, 2, 3, 4$. They are decaying solutions in the half space $z > 0$. In our model, $\tilde{k}_z$ turns out to be doubly degenerate, as shown in Fig. 2. The wave function inside TI ($z > 0$) then has the form

$$\hat{\Phi}_{TI} = \sum_\nu t_\nu e^{i\tilde{k}_z^\nu z}\hat{\phi}_\nu.$$

2.3 Scattering Matrix from Wave-Function Matching

To set the stage for discussing scattering off a topological insulator, it is instructive to recall the generic features of elastic scattering of electrons by a heavy ion with spin-orbit interaction. This classical problem was solved by Mott, and known as *Mott scattering*. The scattering matrix has the general form [**?**]

$$\hat{S}_{Mott} = u\hat{1} + w\hat{\boldsymbol{\sigma}} \cdot (\mathbf{k}_i \times \mathbf{k}_o),$$

where $\mathbf{k}_i$ and $\mathbf{k}_o$ are the incident and outgoing momentum respectively, $\hat{\boldsymbol{\sigma}}$ is the Pauli matrix, and u, w depend on the scattering angle. It is customary to define the spin-flip amplitude $f = S_{21}$, and spin-conserving amplitude $g = S_{11}$. Both f and g are complex numbers, their relative phase defines the *spin rotation angle* $\alpha = \mathrm{Arg}(g^* f)$. One immediately sees that for back scattering, $\hat{S}_{Mott} = u\hat{1}$, so there is no spin flip, $f = 0$. As we will show below, this also holds true for scattering off TI.

Now consider an electron coming from the metal with momentum $\mathbf{k}$ incident on the M-TI interface located at $z = 0$, as schematically shown in Fig. 1(a). We assume the interface is translationally invariant, so the transverse momentum $\mathbf{k}_\parallel = (k_x, k_y)$ is conserved, and

the energy E of the electron lies within the band gap of TI. Then, only total reflection is possible, but the spin-orbit coupling inside TI acting like a $\mathbf{k}$-dependent magnetic field rotates the spin of the incident particle. The scattering (reflection) matrix has the form

$$\hat{S}(\mathbf{k}) = \begin{pmatrix} g & \bar{f} \\ f & \bar{g} \end{pmatrix},$$

where $|g|^2 + |f|^2 = 1$. Our goal is to find the dependence of the scattering amplitudes f, g on $\mathbf{k}$, or equivalently, on energy E and incident angle θ. From time-reversal symmetry, $\bar{f}(E,\theta) = f(E,-\theta)$ and $\bar{g}(E,\theta) = g(E,-\theta)$. We shall show that $f(\mathbf{k}_\parallel) = -f(-\mathbf{k}_\parallel)$, $g(\mathbf{k}_\parallel) = g(-\mathbf{k}_\parallel)$. So f is an odd function of θ, while g is even in θ. Since our problem can be viewed as coherent multiple scattering from a lattice array of Mott scatters occupying half the space, we will refer to spin-active scattering at the metal-TI interface as Mott scattering.

Consider a spin up electron from the conduction band of the metal with momentum $\mathbf{k}$ and energy $E = \epsilon_0(\mathbf{k}) - E_F - d_0(\mathbf{k})$ lying within the band gap of TI. The wave function inside the metal ($z < 0$) has the form

$$\hat{\Phi}_M = (r_1 e^{-ik'_z z}, r_2 e^{-ik'_z z}, e^{ik_z z} + r_3 e^{-ik_z z}, r_4 e^{-ik_z z})^{\mathrm{T}},$$

up to the trivial $e^{i(k_x x + k_y y)}$ and renormalization factor. Here $k_z = \hat{z} \cdot \mathbf{k}$, and $\{r_i\}$ are the reflection amplitudes. We identify the spin flip amplitude $f = r_4$ and the spin-conserving amplitude $g = r_3$. Note that there is no propagating mode at energy E available in the valence band for the reflected electron. So k'_z is purely imaginary. At such energy, there is no propagating mode available in TI. We have discussed the evanescent wave function $\hat{\Phi}_{TI}$ in the previous section. With $\hat{\Phi}_M$ and $\hat{\Phi}_{TI}$, we solve the boundary condition at $z = 0$ to obtain r_ν, t_ν and the scattering matrix S.

Fig. 3 shows the magnitude and phase of f and g versus the incident angle θ for

$E = 0.1$eV, with E_F set to be 0.28eV. At normal incidence, $\theta = 0$, spin flip scattering is forbidden as in the single-ion Mott scattering. With increasing θ the magnitude of g drops continuously. At a critical angle θ_c, $|g|$ drops to zero and we have perfect (100%) spin flip reflection. At the same time, the spin rotation angle α (the relative phase between f and g) jumps by π.

It is tantalizing to think of what happens at θ_c as resonant scattering with the helical surface mode of the TI. This however is problematic. We are considering good contacts at which the wave functions of the two materials hybridize strongly. Surface mode is preempted by MIGS. Indeed, we checked that the corresponding critical transverse momentum $k_{\|}$ depends only weakly on E. This is at odds with the linear dispersion of the TI surface mode, $E = A_2 k_{\|}$ [**?**]. To gain better understanding, we now switch to a lattice model to systematically study the role of interface transparency and metal Fermi surface parameter (E_f, k_f, v_f) on the scattering matrix.

2.4 Interface Spectrum and Scattering Matrix from Lattice Green Function

We consider a simple lattice model for the M-TI junction. The topological insulator is modeled by a tight binding Hamiltonian on cubic lattice,

$$\mathscr{H}_R = \sum_{k_+,n} \Big\{ \hat{\psi}^\dagger_{k_+,n} (b_1 \hat{\Gamma}_0 - i\tfrac{a_1}{2} \hat{\Gamma}_3) \hat{\psi}_{k_+,n+1} + h.c.$$

$$+ \hat{\psi}^\dagger_{k_+,n} \left[d(k_+) \hat{\Gamma}_0 + a_2 (\hat{\Gamma}_1 \sin k_x + \hat{\Gamma}_2 \sin k_y) \right] \hat{\psi}_{k_+,n} \Big\}.$$

Here $\hat{\psi} = (\psi_{+\uparrow}, \psi_{+\downarrow}, \psi_{-\uparrow}, \psi_{-\downarrow})^{\mathrm{T}}$ is the annihilation operator, $d(k_+) = M - 2b_1 + 2b_2(\cos k_x + \cos k_y - 2)$ with k measured in $1/a$. The cubic lattice consists of layers of square lattice stacked in the z direction, n is the layer index, and k_+ is the momentum in the xy plane. The isotropic version of $\mathscr{H}_R$, with $a_1 = a_2$, $b_1 = b_2$, was studied by Qi et al as a minimal model

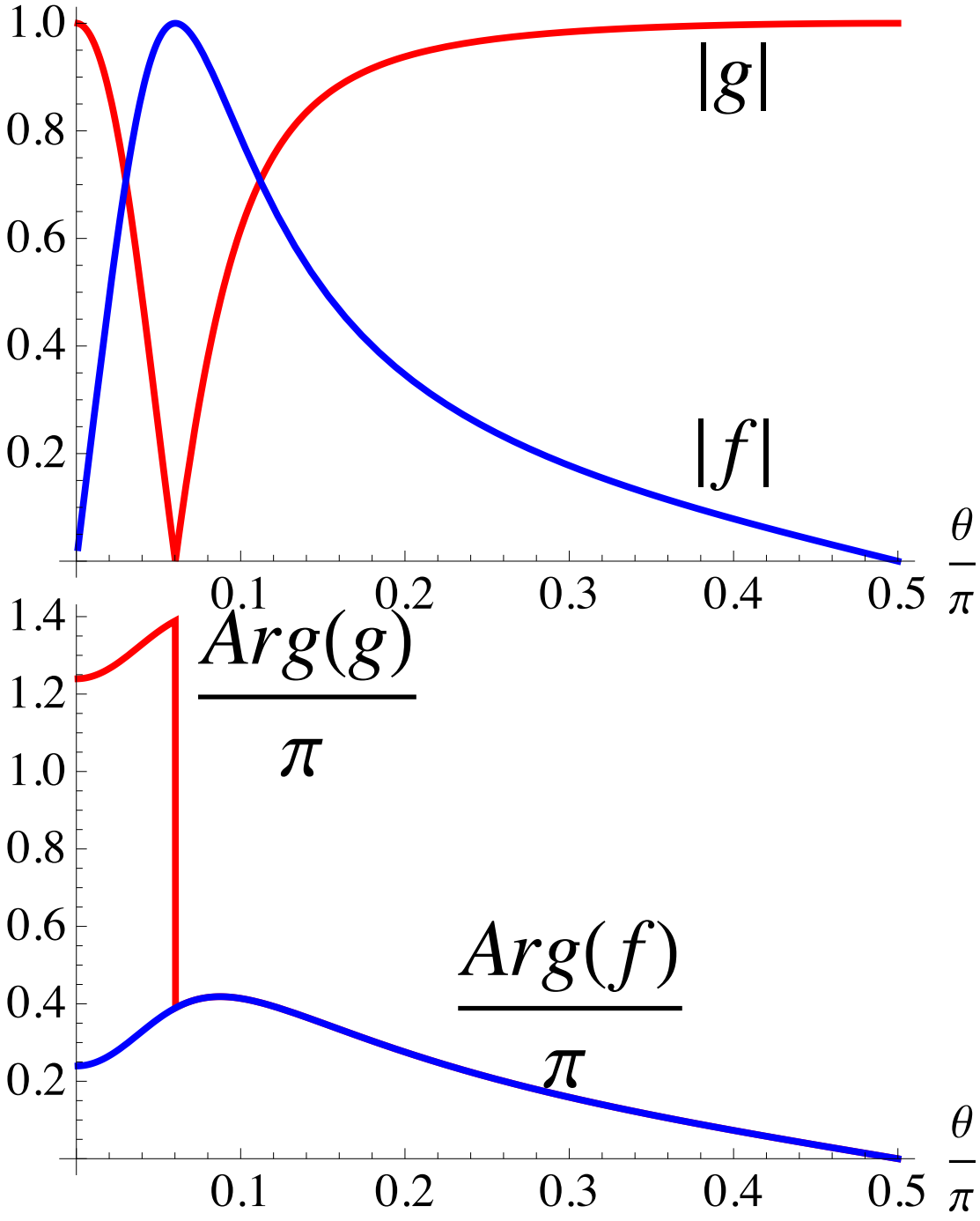

Figure 2.3: The magnitudes (upper panel) and the phases (lower panel) of the spin-flip amplitude f and spin-conserving amplitude g versus the incident angle θ. $E = 0.1$eV, E_F=0.28eV. $|g|^2 + |f|^2 = 1$. Arg(g) and Arg(f) are shifted upward by π for clarity.

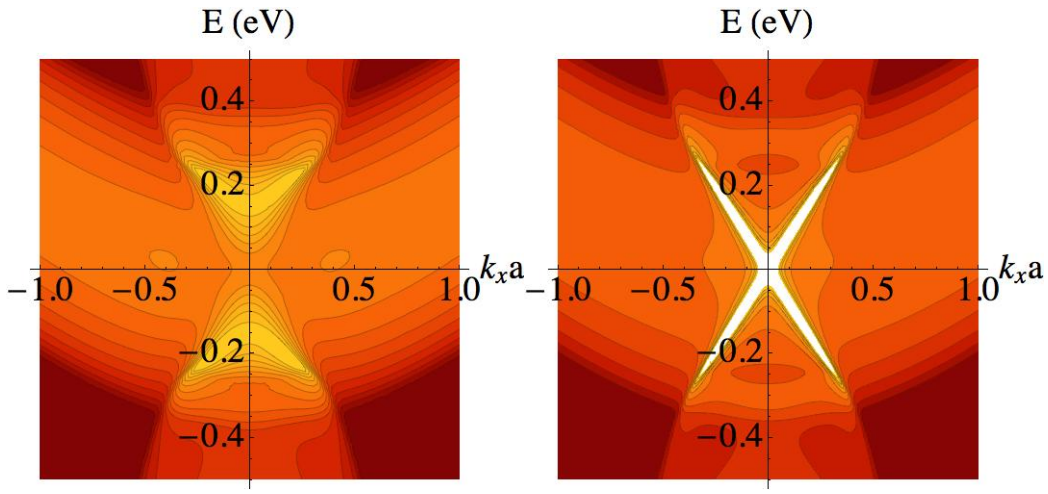

Figure 2.4: The spectral function $N(E, k_x, k_y = 0)$ at the interface of metal and topological insulator. Left: good contact, $J = t_M$, showing the continuum of metal induced gap states. Right: poor contact with low transparency, $J = 0.2t_M$, showing well defined Dirac spectrum as on the TI surface. $t_M = 0.18eV$, $\mu_M = -4t_M$, a is lattice spacing.

for 3D topological insulators [**?**]. To mimic Bi_2Se_3, we set the lattice spacing $a = 5.2$Å, which gives the correct unit cell volume, and $a_i = A_i/a$, $b_i = B_i/a^2$ for $i = 1, 2$. Although a crude caricature of the real material, $\mathscr{H}_R$ yields the correct gap size and surface dispersion, it also reduces to the continuum $\mathbf{k} \cdot \mathbf{p}$ Hamiltonian $\hat{H}_{TI}$ in the small k limit, aside from the topologically trivial $\epsilon_0(\mathbf{k})$ term.

As a generic model for metal, we consider a single band tight binding Hamiltonian on cubic lattice,

$$\mathscr{H}_L = \sum_{k_+,n,\sigma} [h(k_+) n_{k_+,n,\sigma} - t_M \phi^\dagger_{k_+,n,\sigma} \phi_{k_+,n+1,\sigma} + h.c.]$$

where $h(k_+) = -2t_M(\cos k_x + \cos k_y) - \mu_M$. The Fermi surface parameters of the metal can be varied by tuning t_M and μ_M. The metal occupies the left half space, $n \leq 0$, and the TI occupies the right half space $n \geq 1$. The interface domain consists of layer $n = 0, 1$. The coupling between metal and TI is described by hopping,

$$\mathscr{H}_{LR} = -\sum_{k_+,\ell,\sigma} J_\ell \psi^\dagger_{k_+,n=1,\ell,\sigma} \phi_{k_+,n=0,\sigma} + h.c.$$

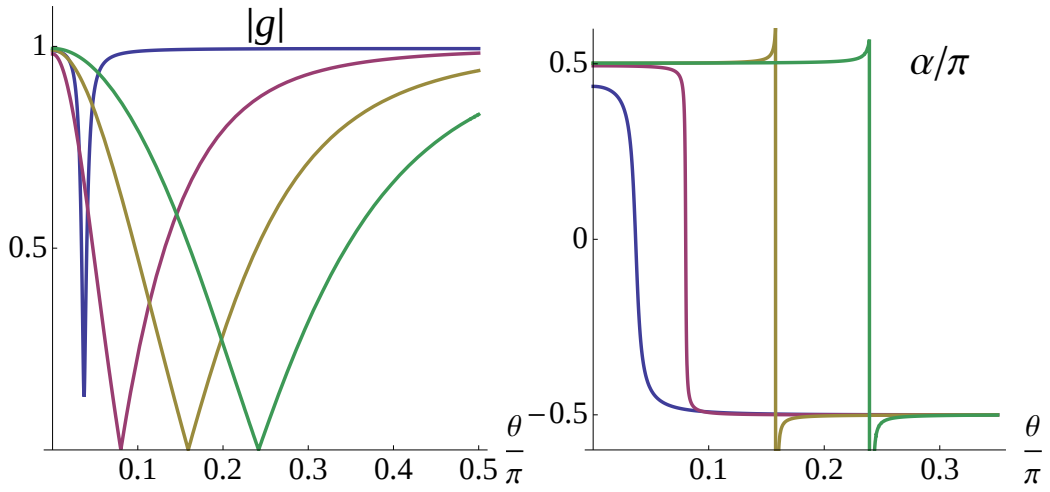

Figure 2.5: The spin-conserving reflection amplitude $|g|$ and spin rotation angle α versus the incident angle θ for increasing contact transparency, $J/t_M = 0.25, 1, 1.5, 2$ (from left to right). $t_M = 0.18eV$, $\mu_M = -4t_M$, $E = 0.05$eV, $k_y = 0$. $|f|^2 = 1 - |g|^2$.

J_ℓ is the overlap integral between the p-orbital $\ell = \pm$ of TI and the s-like orbital of metal. For simplicity, we assume J_ℓ is independent of spin. Then, $J_+ = -J_- = J$. J can be tuned from weak to strong. Small J mimics a large tunneling barrier between M and TI, and large J (comparable to t_M or B_2) describes a good contact.

The lattice Green function of the composite system is computed via standard procedure by introducing the inter-layer transfer matrix and the method of interface Green function matching [**?**]. Fig. 4 shows two examples of the local spectral function (momentum-resolved density of states) at the interface,

$$N(E, k_+) = -\sum_{n=0,1} \mathrm{Im}\mathrm{Tr}\hat{\mathscr{G}}(E, k_+)_{n,n},$$

where $\hat{\mathscr{G}}(E, k_+)_{n,n'}$ is the local Green function at the interface with $n, n' = 0, 1$, and the trace is over the spin and orbital space. In the tunneling (weak coupling, small J) limit, the interface spectrum includes a sharply defined Dirac cone as on the surface of TI. As J is increased, the linearly dispersing mode becomes ill defined and eventually replaced by a continuum of metal induced gap states.

Once the lattice Green function is known for given incident E and $k_{\|}$, the scattering (reflection) matrix can be constructed from $\hat{\mathscr{G}}$ by [**?**],

$$\hat{S}(E, k_+) = \hat{\mathscr{G}}(E, k_+)_{0,0} g_M^{-1}(E, k_+) - \hat{1}$$

where g_M is the spin-degenerate bulk Green function of metal. Fig. 5 shows the evolution of $|g(\theta)|$ and $\alpha(\theta)$ for increasing J, where a level broadening of $E/10$ is used. Most importantly, we observe that the existence of a critical angel θ_c, where complete spin-flip occurs and α jumps by π, is a robust phenomenon. It is independent of the details of the contact, the metal Fermi surface, or other high energy features in the band structure.

To understand the perfect spin flip, we first focus on the tunneling limit, $J \ll t_M$. In this limit, the local spectrum at layer $n = 1$ as shown in the right panel of Fig. 4 approaches the TI surface spectrum, namely the helical Dirac cone. An incident up spin tunneling across the barrier will develop resonance with the helical mode, which is a quasi-stationary state with long life time, if its momentum and energy satisfy $k_{\|} = E/A_2$. Moreover, it has to flip its spin, since only down spin can propagate in the k_x direction (suppose $k_y = 0$). The π jump in the phase shift is also characteristic of the resonance. Indeed, we have checked that precisely at θ_c the resonance criterion, $k_f \sin\theta_c = E/A_2$, is met. We also varied μ_M for fixed J and t_M, bigger μ_M yields a bigger Fermi surface and a smaller θ_c. This is consistent with the resonance criterion above.

As J is increased, the width of the resonance grows and eventually it is replaced by a broad peak (dip) in $|f|$ ($|g|$), but the vanishing of $|g|$ and π shift in α at θ_c persist to good contacts, even though in this limit the interface is flooded by MIGS (left panel of Fig. 4) and bears little resemblance to the Dirac spectrum. With all other parameters held fixed, θ_c increases with J. Qualitatively, coupling to TI renormalizes the metal spectrum near the interface, producing a smaller effective k_f (hence a larger θ_c) compared to its bulk value. It is remarkable that perfect spin flip at the critical angle persists all the way from poor to good contacts. Indeed, the main features observed here for for good contacts using

the lattice model agree well with the results obtained in previous section by wave function matching.

2.5 Discussions

We now discuss the experimental implications of our results. The M-TI interface spectrum can be measured by ARPES (or scanning tunneling microscope) experiments on metal film coated on a topological insulator. Our results also suggest that a topological insulator can serve as a perfect mirror to flip the electron spin in metal. Such spin-active scattering at the M-TI interface may be exploited to make novel spintronic devices. The magnitude of g or f can be measured by attaching two ferromagnetic leads to a piece of metal in contact with TI, forming a multi-terminal device. One of the ferromagnetic leads produces spin-polarized electrons incident on the M-TI interface at some angle, while the other lead detects the polarization of reflected electron, as in a giant magneto-resistance junction. The spin rotation angle α can be measured indirectly by comparing the predicted current-voltage characteristics of M-TI-M or Superconducto-TI-Superconductor junctions, which are sensitive the phase shift α. It can also be inferred from the spin transport in a TI-M-TI sandwich, as discussed for QSH insulator in Ref. [**?**]. Detailed calculations of the transport properties of these structured, using the scattering matrix obtained here, will be subjects of future work.

Chapter 3: Superconducting Proximity Effect

We present microscopic, self-consistent calculations of the superconducting order parameter and pairing correlations near the interface of an s-wave superconductor and a three-dimensional topological insulator with spin-orbit coupling. We discuss the suppression of the order parameter by the topological insulator and show that the equal-time pair correlation functions in the triplet channel, induced by spin-flip scattering at the interface, are of $p_x \pm ip_y$ symmetry. We verify that the spectrum at sub-gap energies is well described by the Fu-Kane model. The sub-gap modes are viewed as interface states with spectral weight penetrating well into the superconductor. We extract the phenomenological parameters of the Fu-Kane model from microscopic calculations, and find they are strongly renormalized from the bulk material parameters. This is consistent with previous results of Stanescu et al for a lattice model using perturbation theory in the tunneling limit.

3.1 Introduction

Fu and Kane showed that at the interface between a three-dimensional topological band insulator (TI) and an s-wave superconductor (S) forms a remarkable two-dimensional non-Abelian superconductor [**?**]. It hosts Majorana zero modes at vortex cores, as in a $p_x + ip_y$ superconductor [**?**], but respects time-reversal symmetry. As argued in Ref. [**?**], the presence of superconductor induces a pairing interaction between the helical Dirac fermions at the surface of the topological insulator, and gaps out the surface spectrum. Then, the interface can be modeled elegantly by a simple matrix Hamiltonian in Nambu space (we follow the

convention of Ref. [**?**]),

$$H_{FK}(\mathbf{k}) = \begin{pmatrix} h_s(\mathbf{k}) & i\sigma_y\Delta_s \\ -i\sigma_y\Delta_s^* & -h_s^*(-\mathbf{k}) \end{pmatrix}, \tag{3.1}$$

where $\mathbf{k} = (k_x, k_y)$ is the two-dimensional momentum in the interface plane, σ_i are the Pauli matrices, $h_s(\mathbf{k})$ is the surface Hamiltonian for the topological insulator describing the helical Dirac fermions [**?**, **?**],

$$h_s(\mathbf{k}) = -\mu_s + v_s(\sigma_x k_y - \sigma_y k_x). \tag{3.2}$$

Fu and Kane also proposed to use S-TI proximity structures to generate and manipulate Majorana fermions which obey non-Abelian statistics and are potentially useful for fault tolerant quantum computation [**?**]. This proposal and a few others that followed based on superconductor-semiconductor heterostructures [**?**, **?**, **?**, **?**, **?**] have revived the interest in superconducting proximity effect involving insulating/semiconducting materials with spin-orbit coupling. More complex S-TI proximity structures with ferromagnets [**?**, **?**] or unconventional superconductors [**?**] have been investigated.

Experiments are beginning to realize various S-TI proximity structures [**?**, **?**, **?**]. In light of these developments, it is desirable to understand to what extent the effective model H_{FK} holds, and what are the values of (Δ_s, μ_s, v_s) for given materials. Answering these questions is crucial for future experiments designed to probe and manipulate Majorana fermions. As a first step in this direction, Stanescu et al considered a microscopic lattice model for the TI-S interface [**?**]. In this model, TI and S are described by a tight binding Hamiltonian defined on the diamond and hexagonal lattice respectively. The two materials are coupled by tunneling term in the Hamiltonian. These authors found that for small $\mathbf{k}$, $H_{FK}(\mathbf{k})$ is valid but its parameters are significantly renormalized by the presence of the superconductor. This is supported by leading order perturbation theory in the weak coupling (tunneling) limit.

They also discussed the induced p-wave correlation within the framework of perturbation theory. The p-wave correlation has also been noted in an analogous proximity structure in two dimension between a quantum spin Hall insulator and a superconductor [**?**].

In this work, we consider S-TI proximity structures where S and TI are *strongly* coupled to each other, rather than being separated by a tunneling barrier. This is the desired, presumably the optimal, configuration to realize the Fu-Kane proposal, e.g. to achieve maximum value of Δ_s in H_{FK} for given superconductor. In the strong coupling limit, the modification of superconductivity by the TI becomes important. This includes the suppression of the superconducting order parameter, the induction of triplet pair correlations by spin-active scattering at the interface, and the formation of interface states below the bulk superconducting gap. In order to accurately answer questions raised in the preceding paragraph for strongly coupled S-TI structures, one has to self-consistently determine the spatial profile of the order parameter near the interface.

Our work is also motivated by recent experimental discovery that Copper-doped topological insulator $Cu_xBi_2Se_3$ becomes superconducting at a few Kelvins [**?**, **?**, **?**]. It seems possible then to combine such superconductors with topological insulator Bi_2Se_3 to achieve strong proximity coupling. We set up microscopic, continuum models for the S-TI structures and solve the result Bogoliubov-de Gennes (BdG) equation numerically. We first compute the superconducting order parameter as a function of the distance away from the interface. We then verify the validity of the Fu-Kane effective model and extract its parameters from the low energy sector of the energy spectrum. The emergence of H_{FK} will be viewed as the result of the "inverse proximity effect", namely strong modification of superconductivity by the presence of TI. This is in contrast to the previous viewpoint of pairing between surface Dirac fermions, which is a more proper description in the tunneling limit. The spectral weight of these low energy modes (with energy below the bulk superconducting gap) are shown explicitly to peak near the interface but penetrate well into the superconductor. We will also show analytically that the induced triplet pair correlations are of $p_x \pm ip_y$ orbital symmetry, and systematically study their spatial and momentum dependence. Our results

connect the phenomenological theory of Fu and Kane [**?**] to real materials. Our results for continuum models and strong coupling limit are also complementary to the results of Stanescu et al [**?**] for lattice models and tunneling limit.

In what follows, we first outline the formulation of the problem and then present the main results. Technical details on numerically solving the BdG equation are relegated to the appendix.

3.2 Model and Basic Equations

The band gaps of topological insulators are much larger than the superconducting gap of all weak coupling s-wave superconductors. For the purpose of studying the proximity effect between such superconductors and topological insulators, it is sufficient to describe the topological insulator using the low energy effective $\mathbf{k}\cdot\mathbf{p}$ Hamiltonian. Following Zhang et al [**?**], we model Bi_2Se_3 by

$$H_{TI}(\mathbf{k}) = \begin{pmatrix} M(\mathbf{k}) & 0 & A_1 k_z & A_2 k_- \\ 0 & M(\mathbf{k}) & A_2 k_+ & -A_1 k_z \\ A_1 k_z & A_2 k_- & -M(\mathbf{k}) & 0 \\ A_2 k_+ & -A_1 k_z & 0 & -M(\mathbf{k}) \end{pmatrix} - \mu \hat{I}. \tag{3.3}$$

Here $k_\pm = k_x \pm i k_y$, $M(\mathbf{k}) = M - B_1 k_z^2 - B_2(k_x^2 + k_y^2)$, and $\hat{I}$ is 4×4 unit matrix. The numerical values of the parameters are obtained from first principle calculations [**?**, **?**], $M = 0.28$ eV, $A_1 = 2.2$ eVÅ, $A_2 = 4.1$ eVÅ, $B_1 = 10$ eVÅ^2, $B_2 = 56.6$ eVÅ^2. We work in basis $\{|1\uparrow\rangle, |1\downarrow\rangle, |2\uparrow\rangle, |2\downarrow\rangle\}$, where 1 (2) labels the $P1_z^+$ ($P2_z^+$) orbital [**?**]. Note that we have neglected the unimportant diagonal term $\epsilon_0(\mathbf{k})$ in Ref. [**?**] which only slightly modifies the overall curvature of the band dispersion. We also keep the chemical potential μ as a tuning parameter.

We consider a simple model of superconductor derived from a metallic state obtained

by turning off the spin-orbit coupling ($A_1 = A_2 = 0$) in H_{TI} and tuning the Fermi level well into the conduction band [**?**]. The metal Hamiltonian

$$H_M(\mathbf{k}) = \mathrm{diag}[M(\mathbf{k}), M(\mathbf{k}), -M(\mathbf{k}), -M(\mathbf{k})] - E_f\hat{I}, \tag{3.4}$$

with $E_f > M$. This mimics electron-doping the topological insulator [**?**] or equivalently electrochemically shifting its chemical potential by applying a gate voltage [**?**]. As shown in Fig. 3.1, the valence band (band 1 with dispersion $M(\mathbf{k}) - E_f$) is well below the Fermi level and remains inert as far as superconductivity is concerned. Next, within the framework of Bardeen-Cooper-Schrieffer theory, we assume attractive interaction between the electrons in the conduction band (band 2) near the Fermi surface described by the reduced Hamiltonian,

$$H_{int} = \sum_{\mathbf{k}} \psi^\dagger_{2\uparrow}(\mathbf{k})\psi^\dagger_{2\downarrow}(-\mathbf{k})\Delta + h.c. \tag{3.5}$$

Here Δ is the superconducting order parameter, $\psi^\dagger_{l\sigma}$ is the electron creation operator for orbital $l = 1, 2$ and spin $\sigma =\uparrow, \downarrow$. The superconductor is then described by

$$H_S = \sum_{\mathbf{k},l,\sigma} \psi^\dagger_{l\sigma}(\mathbf{k})H_M(\mathbf{k})_{l\sigma,l\sigma}\psi_{l\sigma}(\mathbf{k}) + H_{int}. \tag{3.6}$$

Note that H_S and H_{TI} are in the same basis.

This model can serve as a generic model for s-wave superconductors with negligible spin-orbital coupling. Whether it can actually describe the superconductor $Cu_xBi_2Se_3$ has to be settled by future experiments. The transition temperature of $Cu_xBi_2Se_3$ at optimal doping $x = 0.12$ is $T_c = 3.8$K, which corresponds to a zero temperature superconducting gap $\Delta \sim 0.6$meV [**?**, **?**, **?**]. The Fermi level is 0.25eV above the bottom of the conduction band, and the Fermi wave vector $k_f \sim 0.12\text{Å}^{-1}$. The pairing symmetry of $Cu_xBi_2Se_3$ is to our best knowledge is unknown at present (it appears to be fully gapped from the specific

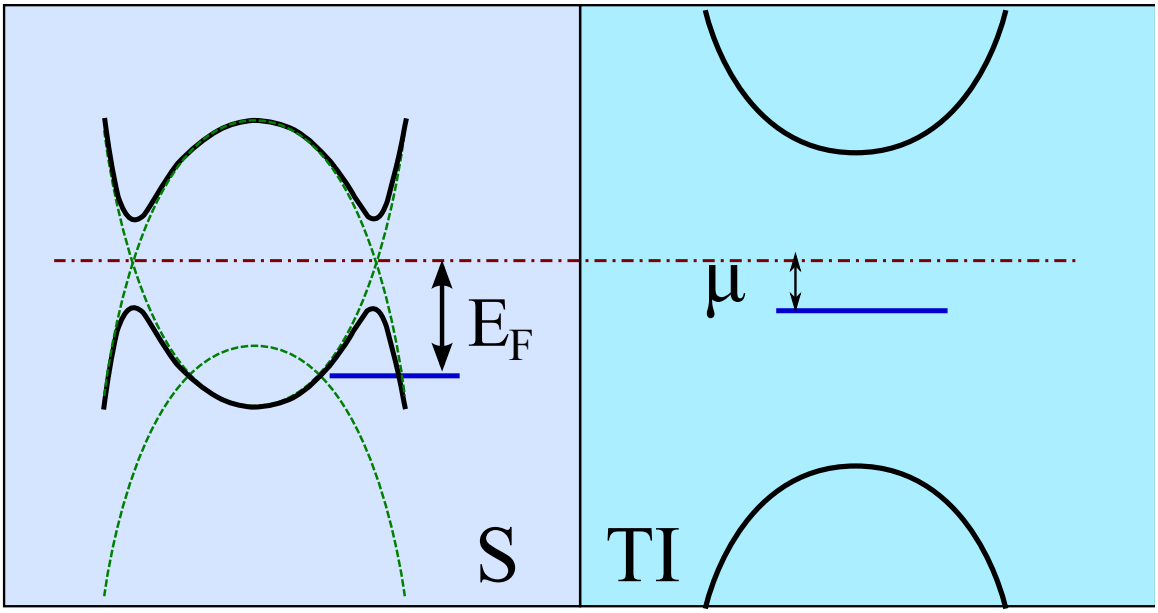

Figure 3.1: Schematic (not to scale) band diagrams in a superconductor-topological insulator (S-TI) proximity structure. E_f is the Fermi energy of the metal described by H_M measured from the band crossing point. μ is the chemical potential of TI measured from the band gap center. The superconducting gap is much smaller than the band gap of TI.

heat measurement [**?**] and might be a topological superconductor [**?**]). If it turns out to be a conventional s-wave superconductor, its mains features will be captured by H_S above with suitable choice of E_f and Δ.

Now consider a proximity structure consisting of a superconductor at $z < d$ and a topological insulator at $z > d$ (Fig. 3.1). The interface at $z = d$ is assumed to be specular, so the momentum $\mathbf{k}_{\|} = (k_x, k_y)$ parallel to the interface is conserved. The Hamiltonian for

the whole system

$$\mathcal{H} = \int d\mathbf{k}_\parallel dz \Big\{ \sum_\sigma \psi^\dagger_{1\sigma}(\mathbf{k}_\parallel, z)[h_0 - \mu(z)]\psi^\dagger_{1\sigma}(\mathbf{k}_\parallel, z)$$

$$- \sum_\sigma \psi^\dagger_{2\sigma}(\mathbf{k}_\parallel, z)[h_0 + \mu(z)]\psi^\dagger_{2\sigma}(\mathbf{k}_\parallel, z)$$

$$+ \Delta(z)\psi^\dagger_{2\uparrow}(\mathbf{k}_\parallel, z)\psi^\dagger_{2\downarrow}(-\mathbf{k}_\parallel, z) + h.c.$$

$$+ A_1(z)[\psi^\dagger_{1\uparrow}(-i\partial_z)\psi_{2\uparrow} + \psi^\dagger_{1\downarrow}(i\partial_z)\psi_{2\downarrow} + h.c.]$$

$$+ A_2(z)[\psi^\dagger_{1\uparrow}k_-\psi_{2\downarrow} + \psi^\dagger_{1\downarrow}k_+\psi_{2\uparrow} + h.c.]\Big\}. \tag{3.7}$$

Here $h_0(\mathbf{k}_\parallel, \partial_z) = M - B_1\partial_z^2 - B_2 k_\parallel^2$, $\mu(z)$ and $A_i(z)$ are piece-wise constant,

$$\mu(z) = E_f\theta(d - z) + \mu\theta(z - d), \tag{3.8}$$

$$A_i(z) = A_i\theta(z - d), \;\; i = 1, 2 \tag{3.9}$$

in terms of the step function θ. The order parameter obeys the gap equation

$$\Delta(z) = g(z) \int d\mathbf{k}_\parallel \langle \psi_{2\uparrow}(\mathbf{k}_\parallel, z)\psi_{2\downarrow}(-\mathbf{k}_\parallel, z)\rangle. \tag{3.10}$$

We assume $g(z) = g\theta(d - z)$, the coupling constant g determines the bulk gap.

To self-consistently solve Eq. (3.7) and (3.10), we introduce Bogoliubov transformation

$$\psi_{l\sigma}(\mathbf{k}_\parallel, z) = \sum_n u_{n,l\sigma}(\mathbf{k}_\parallel, z)\gamma_{n,\mathbf{k}_\parallel} + v^*_{n,l\sigma}(\mathbf{k}_\parallel, z)\gamma^\dagger_{n,\mathbf{k}_\parallel} \tag{3.11}$$

to diagonalize $\mathcal{H}$ as

$$\mathcal{H} = E_g + \int d\mathbf{k}_\parallel \sum_n \epsilon_n(k_\parallel)\gamma^\dagger_{n,\mathbf{k}_\parallel}\gamma_{n,\mathbf{k}_\parallel}, \tag{3.12}$$

where E_g is the ground state energy, and $\gamma^\dagger_{n,\mathbf{k}_\parallel}$ is the creation operator of Bogoliubov quasi-particles with energy $\epsilon_n(k_\parallel)$. The wave function u and v satisfy the following Bogliubov-de Gennes (BdG) equation,

$$\hat{H}_B(\mathbf{k}_\parallel, z)\hat{\phi}_n(\mathbf{k}_\parallel, z) = \epsilon_n(k_\parallel)\hat{\phi}_n(\mathbf{k}_\parallel, z). \tag{3.13}$$

Here, the BdG Hamiltonian

$$\hat{H}_B = \begin{pmatrix} h_0 - \mu & \mathbf{d}\cdot\boldsymbol{\sigma} & 0 & 0 \\ \mathbf{d}\cdot\boldsymbol{\sigma} & -h_0 - \mu & 0 & -\Delta\, i\sigma_y \\ 0 & 0 & \mu - h_0 & \mathbf{d}\cdot\boldsymbol{\sigma}^* \\ 0 & \Delta^*\, i\sigma_y & \mathbf{d}\cdot\boldsymbol{\sigma}^* & \mu + h_0 \end{pmatrix}, \tag{3.14}$$

and the wave function (dropping the arguments)

$$\hat{\phi}_n = (u_{n,1\uparrow}, u_{n,1\downarrow}, u_{n,2\uparrow}, u_{n,2\downarrow}, v_{n,1\uparrow}, v_{n,1\downarrow}, v_{n,2\uparrow}, v_{n,2\downarrow})^{\mathrm{T}}. \tag{3.15}$$

The vector $\mathbf{d}(\mathbf{k}_\parallel, z)$ is defined as

$$d_x = A_1(z)k_x,\ d_y = A_1(z)k_y,\ d_z = A_2(z)(-i\partial_z). \tag{3.16}$$

Other quantities such as $h_0(\mathbf{k}_\parallel, z)$, $\mu(z)$, and $\Delta(z)$ are defined above. In terms of the wave functions, the zero temperature gap equation becomes

$$\Delta(z) = g(z)\int d\mathbf{k}_\parallel \sum_n{}' u_{n,2\uparrow}(\mathbf{k}_\parallel, z)v^*_{n,2\downarrow}(-\mathbf{k}_\parallel, z), \tag{3.17}$$

where the summation denoted by prime is restricted to $0 < \epsilon_n < \omega_D$ with ω_D being the Debye frequency.

We will exploit a particular symmetry of the BdG Hamiltonian to simplify calculations. Define the polar angle φ_k for the in-plane wave vector $\mathbf{k}_\parallel$,

$$k_x + ik_y = k_\parallel e^{i\varphi_k}. \tag{3.18}$$

Then the BdG Hamiltonian for arbitrary (k_x, k_y) is related to that for $(k_x = k_\parallel, k_y = 0)$ by unitary transformation

$$\hat{U}^\dagger(\mathbf{k}_\parallel)\hat{H}_B(k_x, k_y)\hat{U}(\mathbf{k}_\parallel) = \hat{H}_B(k_\parallel, 0). \tag{3.19}$$

Here U is a block diagonal matrix,

$$U(\mathbf{k}_\parallel) = \mathrm{diag}[e^{-i\sigma_z \frac{\varphi_k}{2}}, e^{-i\sigma_z \frac{\varphi_k}{2}}, e^{i\sigma_z \frac{\varphi_k}{2}}, e^{i\sigma_z \frac{\varphi_k}{2}}]. \tag{3.20}$$

Thus, the eigen energy ϵ_n only depends on the magnitude of $\mathbf{k}_\parallel$. Once the wave function for $\varphi_k = 0$ is known, the wave function for $\varphi_k \in (0, 2\pi)$ can be obtained by simple unitary transformation.

We solve the matrix differential equation (3.13) by conserving it into an algebraic equation, following the treatment of superconductor-ferromagnet structure by Halterman and Valls [**?**]. The whole S-TI proximity structure is assumed to have finite dimension L in the z direction. The superconductor occupies the region $0 < z < d$, while the topological insulator occupies $d < z < L$. Hard wall boundary conditions are enforced at the end points, $z = 0$ and $z = L$. The exact boundary conditions at the end points only affect the local physics there, provided that the boundaries are sufficiently far away from the S-TI

interface. We expand the wave function and order parameter in Fourier series [**?**],

$$u_{n,l\sigma}(z) = \sum_m u_{nm}^{l\sigma}\,\phi_m(z), \tag{3.21}$$

$$v_{n,l\sigma}(z) = \sum_m v_{nm}^{l\sigma}\,\phi_m(z), \tag{3.22}$$

$$\Delta(z) = \sum_m \Delta_m\,\phi_m(z), \tag{3.23}$$

$$\phi_m(z) = \sqrt{2/L}\sin(k_m z). \tag{3.24}$$

The integer $m = 1, 2, ..., N$ labels the quantized longitudinal (along z) momentum $k_m = m\pi/L$. The cutoff N is chosen as [**?**]

$$B_1 k_N^2 = M + E_f + \omega_D. \tag{3.25}$$

By expansion Eq. (3.21)-(3.23), the BdG equation becomes an $8N \times 8N$ matrix equation. With a reasonable guess of the order parameter profile, the eigen energies and eigen wave functions are obtained by solving the matrix eigen value problem. Then a new order parameter profile is computed from the gap equation. The procedure is iterated until convergence is achieved. Relevant technical details can be found in the Fourier calculations section.

To analyze the spectrum of the system, it is convenient to define the retarded Green's function

$$G_{l\sigma}^R(\mathbf{k}_\parallel, z, t) = -i\theta(t)\langle\{\psi_{l\sigma}(\mathbf{k}_\parallel, z, t), \psi_{l\sigma}^\dagger(\mathbf{k}_\parallel, z, 0)\}\rangle \tag{3.26}$$

where the time-dependent field operators are in Heisenberg picture. For given $\mathbf{k}_\parallel$ and z, the spectral functions are defined as

$$N_{l\sigma}(\mathbf{k}_\parallel, z, \omega) = -\mathrm{Im}G_{l\sigma}^R(\mathbf{k}_\parallel, z, \omega), \tag{3.27}$$

$$N(\mathbf{k}_\parallel, z, \omega) = \sum_{l\sigma} N_{l\sigma}(\mathbf{k}_\parallel, z, \omega). \tag{3.28}$$

In terms of the wave functions and eigen energies,

$$N_{l\sigma}(\mathbf{k}_{\parallel}, z, \omega > 0) = \sum_{n} |u_{n,l\sigma}(\mathbf{k}_{\parallel}, z)|^2 \delta(\omega - \epsilon_n). \tag{3.29}$$

We also introduce the equal-time pair correlation functions for the conduction electrons

$$F_{\alpha\beta}(\mathbf{k}_{\parallel}, z) = \langle \psi_{2\alpha}(\mathbf{k}_{\parallel}, z) \psi_{2\beta}(-\mathbf{k}_{\parallel}, z) \rangle. \tag{3.30}$$

For example, at zero temperature we have

$$F_{\uparrow\uparrow}(\mathbf{k}_{\parallel}, z) = \sum_{n}{}' u_{n,2\uparrow}(\mathbf{k}_{\parallel}, z) v^{*}_{n,2\uparrow}(-\mathbf{k}_{\parallel}, z), \tag{3.31}$$

$$F_{\downarrow\downarrow}(\mathbf{k}_{\parallel}, z) = \sum_{n}{}' u_{n,2\downarrow}(\mathbf{k}_{\parallel}, z) v^{*}_{n,2\downarrow}(-\mathbf{k}_{\parallel}, z). \tag{3.32}$$

Triplet components of F will be induced near the S-TI interface by spin-active scattering [**?**].

3.3 Fourier Expansion

We follow the numerical scheme of Halterman and Valls to solve the matrix BdG equation [**?**]. The wave functions and the order parameter are expanded in the orthonormal basis $\{\phi_m(z)\}$, with $m = 1, ..., N$. For example, function $u_{n,1\uparrow}(z)$ is represented by N numbers,

$$(u^{1\uparrow}_{n,1}, u^{1\uparrow}_{n,2}, ...u^{1\uparrow}_{n,m}..., u^{1\uparrow}_{n,N}).$$

Accordingly, each term in $\hat{H}_B$ is represented by a $N \times N$ matrix with the matrix elements given by

$$h_0(\mathbf{k}_\parallel, \partial_z) \to \delta_{mm'}(M - B_1 k_m^2 - B_2 k_\parallel^2)$$

$$U(z) \to E_f E_{mm'} + \mu F_{mm'}$$

$$A_2(z)\partial_z \to A_2 G_{mm'}$$

$$A_1(z)k_\pm \to A_z k_\pm F_{mm'}$$

$$\Delta \to D_{mm'} \equiv \sum_{m''} J_{m,m',m''} \Delta_{m''}$$

where

$$E_{mm'} = \int_0^d \phi_m(z)\, \phi_{m'}(z) dz$$

$$F_{mm'} = \int_d^L \phi_m(z)\, \phi_{m'}(z) dz$$

$$G_{mm'} = \int_d^L \phi_m(z) \partial_z \phi_{m'}(z) dz$$

$$J_{m,m',m''} = \int_0^d \phi_m(z)\, \phi_{m'}(z)\, \phi_{m''}(z) dz$$

These integrals can be evaluated analytically. Then the BdG equation becomes an $8N \times 8N$ matrix equation. The gap equation can be rewritten as

$$\Delta_m = g \int d\mathbf{k}_\parallel \sum_n{}' \sum_{m',m''} J_{m,m',m''} u^{2\uparrow}_{nm'}(\mathbf{k}_\parallel) v^{2\downarrow}_{nm''}(-\mathbf{k}_\parallel)^*$$

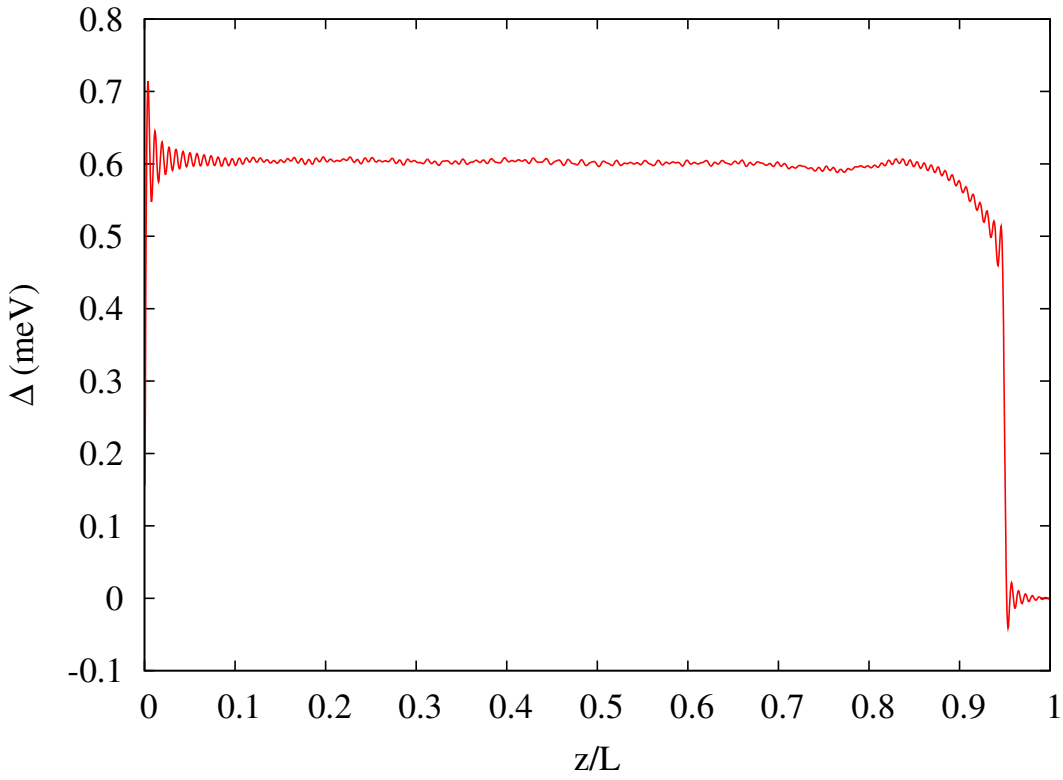

Figure 3.2: The superconducting order parameter $\Delta(z)$ near an S-TI interface at $z = d = 0.95L$. The superconductor occupies $0 < z < d$, and topological insulator occupies $d < z < L$. $L = 300$ nm, μ=0, the bulk gap Δ_0 =0.6meV.

The integral over $\mathbf{k}_{\|}$ is first simplified to an integral over $k_{\|}$ by the symmetry Eq. (3.19) and then evaluated numerically with high momentum cutoff $\sqrt{(E_F + \omega_D + M)/B_2}$.

3.4 The Order Parameter

First we present the spatial profile of the superconducting order parameter $\Delta(z)$ after the convergence is achieved. In all following calculations, E_f is fixed at 0.4eV, which is modeled after optimally doped $Cu_xBi_2Se_3$ [**?**]. And the Debye frequency is set as $\omega_D = 0.1E_f$ [**?**]. Fig. 3.2 shows an example with $\mu = 0$, $L = 300$nm, $d = 0.95L$, and a bulk gap of 0.6meV as found in $Cu_xBi_2Se_3$. Going from the superconductor into the topological insulator, Δ first gets suppressed as the interface is approached before it drops to zero inside TI. The suppression is roughly 20% at the interface. Note that the fine wiggles of Δ in the

simulation results are due to the finite momentum cutoff of the longitudinal momentum k_m. As previously discussed by Stojkovic and Valls [**?**], the number of oscillations is $\sim N/2$, and the oscillation amplitude vanishes in the bulk as N is increased. In this case, N is chosen to be 258 according to Eq. (3.25). So the matrix to be diagonalized is 2064 by 2064.

Fig. 3.3 show the result for $\mu = 0$, $d = 0.9L$, and a superconductor with bulk gap $\Delta_0 \sim$ 2.4meV. Since the coherence length is much smaller than the previous example, it is sufficient to consider $L = 160$nm, and correspondingly $N = 138$. The order parameter profile depends weakly on μ, as shown in Fig. 3.4 for a superconductor with bulk gap ~ 5.2meV. From these examples, one observes that the length scale over which Δ is significantly suppressed does *not* scale with ξ_0, the zero temperature coherence length of the superconductor. Rather it stays roughly the same, on the order of 30nm, as ξ_0 is varied over one decade from Fig. 3.2 to Fig. 3.4 (note the horizontal axis is z/L). This is not very surprising since ξ_0 is not the only length scale at play here. The interface represents a strong (as compared to Δ_0) perturbation that significantly distorts the bulk wave functions. The self-consistent microscopic BdG approach provides a reliable way to capture the details of $\Delta(z)$ near the interface.

It is illuminating to compare the proximity effect in S-TI structure with that in S-F structure [**?**], where F stands for a ferromagnetic insulator. The presence of F breaks time-reversal and spin rotation symmetry and significantly suppresses the order parameter. The suppression is sensitive to the spin mixing angle which is related to the band gap and exchange field of F [**?**]. In contrast, despite the spin-active scattering of electrons by TI which introduces spin-flips and spin-dependent phase shifts [**?**], spin-orbit coupling is not pair breaking. The suppression of Δ near the interface is to a large extent due to the reorganization of local wave functions enforced by the boundary conditions at $z = d$ for piece-wise potentials $\mu(z)$, $A_i(z)$, $g(z)$. It depends on for example how the wave functions decay inside the TI for given E_f and μ, and involves "high-energy" physics beyond the scale of Δ but below the scale of the band gap. To test this, we have investigated the proximity effect between the same superconductor and a hypothetical ordinary insulator modeled by

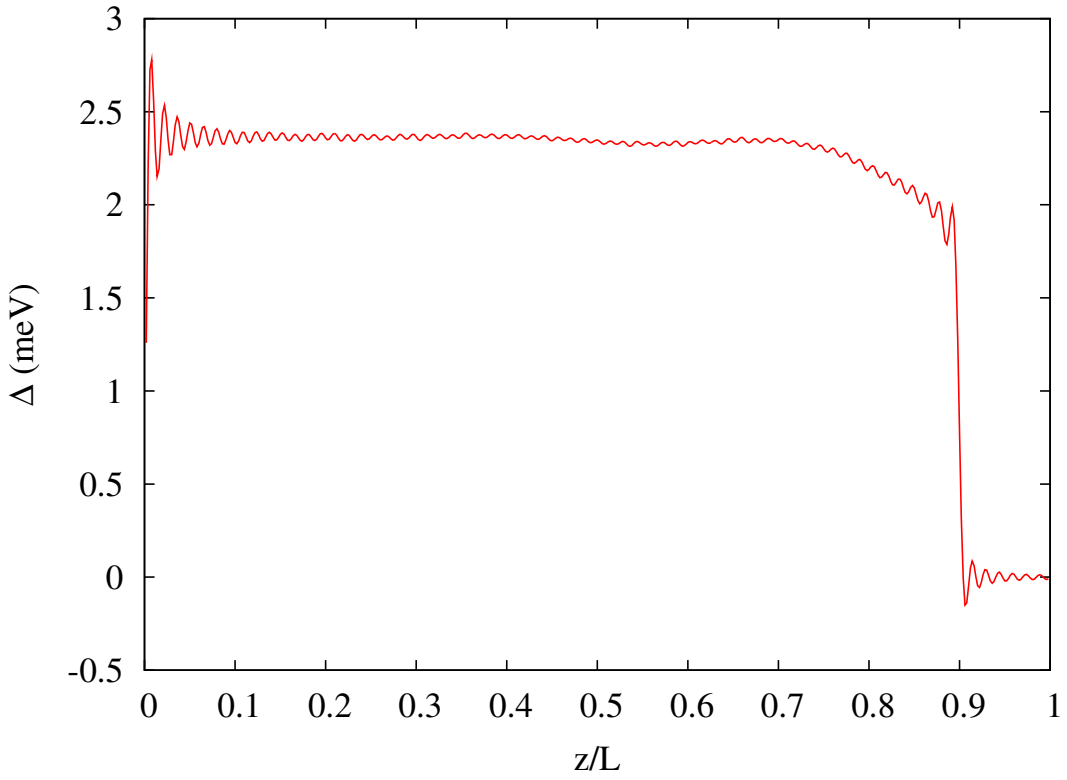

Figure 3.3: The order parameter $\Delta(z)$ near an S-TI interface at $z = d = 0.9L$. $L = 160$ nm, μ=0, $\Delta_0 \sim 2.4$meV.

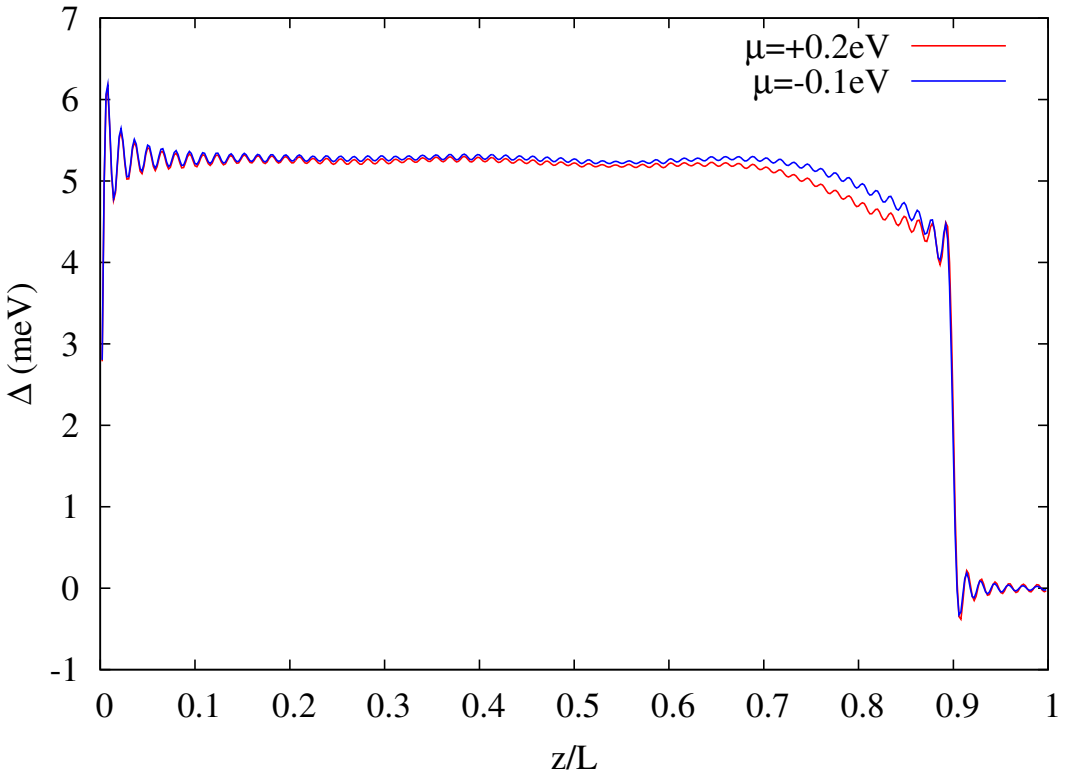

Figure 3.4: The order parameter profile for two different chemical potentials of the topological insulator, $\mu = -0.1$eV and $\mu = 0.2$eV. $L = 160$nm, $\Delta_0 \sim 5.2$meV.

H_{TI} with $A_1 = A_2 = 0$ and the same band gap. The suppression of Δ by such an ordinary insulator turns out to be very similar.

3.5 The Interface Mode and the Fu-Kane Model

Next we analyze the energy spectrum of the system, $\epsilon_n(k_\parallel)$, obtained from the BdG calculation. Take the case of $\mu = 0$, $L = 160$nm, $d = 0.9L$, $\Delta_0 \sim 5.2$meV as an example. Fig. 3.5 shows the first several energy levels of the composite system versus the transverse momentum $k_\parallel$. There are many continuously dispersing modes at energies above the bulk gap. They are the usual Bogoliubov quasiparticles for different quantized longitudinal momenta. One also sees a series of avoided level crossings. At small $k_\parallel$ emerges a well-defined mode below Δ_0. We will identify it as the interface mode first discussed by Fu and Kane [**?**].

The Fu-Kane model Eq. (3.1) predicts the dispersion

$$E(k) = \sqrt{|\Delta_s|^2 + (v_s k \pm \mu_s)^2}. \tag{3.33}$$

We fit the very low energy portion of the spectrum to this prediction to extract the phenomenological parameters in the Fu-Kane model. The result is shown in Fig. 3.5. We find that, not surprisingly, $\Delta_s = 1.8$meV which is much smaller than $\Delta_0 = 5.2$meV, and $v_s = 2.7$eVÅ which deviates significantly from $A_2 = 4.2$eVÅ predicted for the surface dispersion of TI. Moreover, $\mu_s = 7.5$meV despite that the chemical potential of TI is $\mu = 0$. Therefore, our results show that the values of (Δ_s, v_s, μ_s) are strongly renormalized by the presence of the superconductor. This is consistent with the findings of Stanescu et al for weakly coupled S-TI structures [**?**].

We have checked the validity of the Fu-Kane model for a variety of chemical potentials. Representative examples are plotted in Fig. 3.6. In each case, the sub-gap mode can be well accounted by the Fu-Kane model with suitable choice of parameters. While μ_s is always different from μ, numerically we find it scales linearly with μ. At the same time, Δ_s and v_s

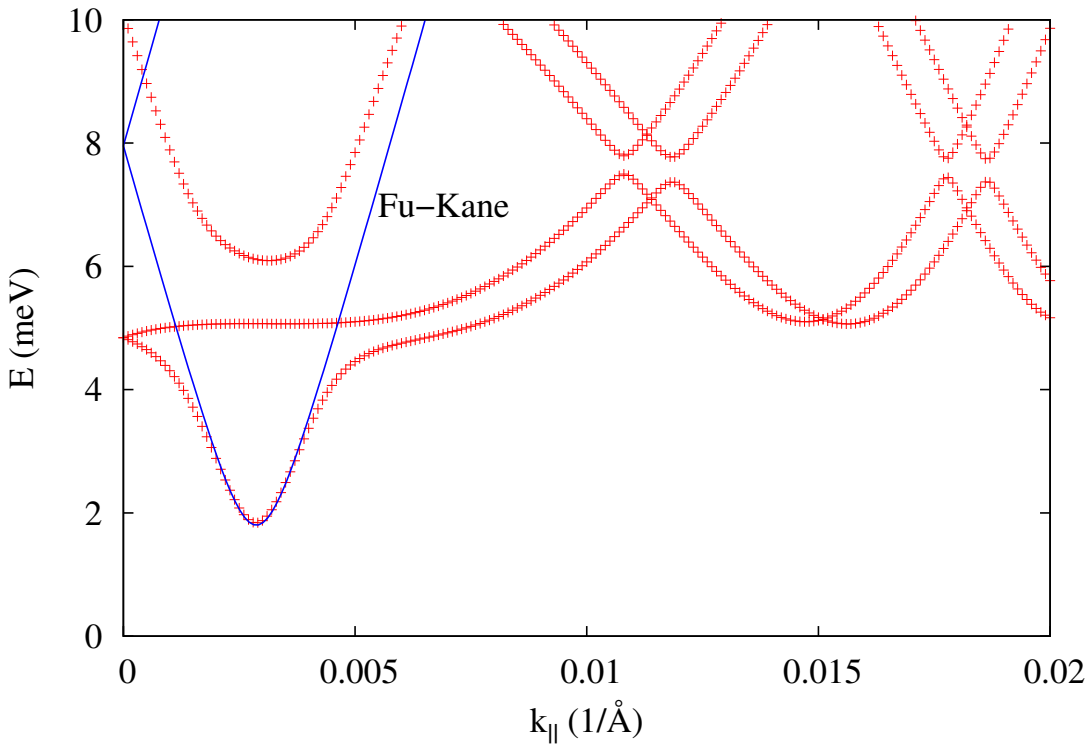

Figure 3.5: The lowest few energy levels $\epsilon_n(k_\parallel)$. $\mu = 0$, $L = 160$nm, and the bulk superconducting gap $\Delta_0 \sim 5.2$meV. A well-defined interface mode is clearly visible at sub-gap energies. Solid lines show a fit to the Fu-Kane model, with $\Delta_s = 1.8$meV, $v_s = 2.7$eVÅ, and $\mu_s = 7.5$meV.

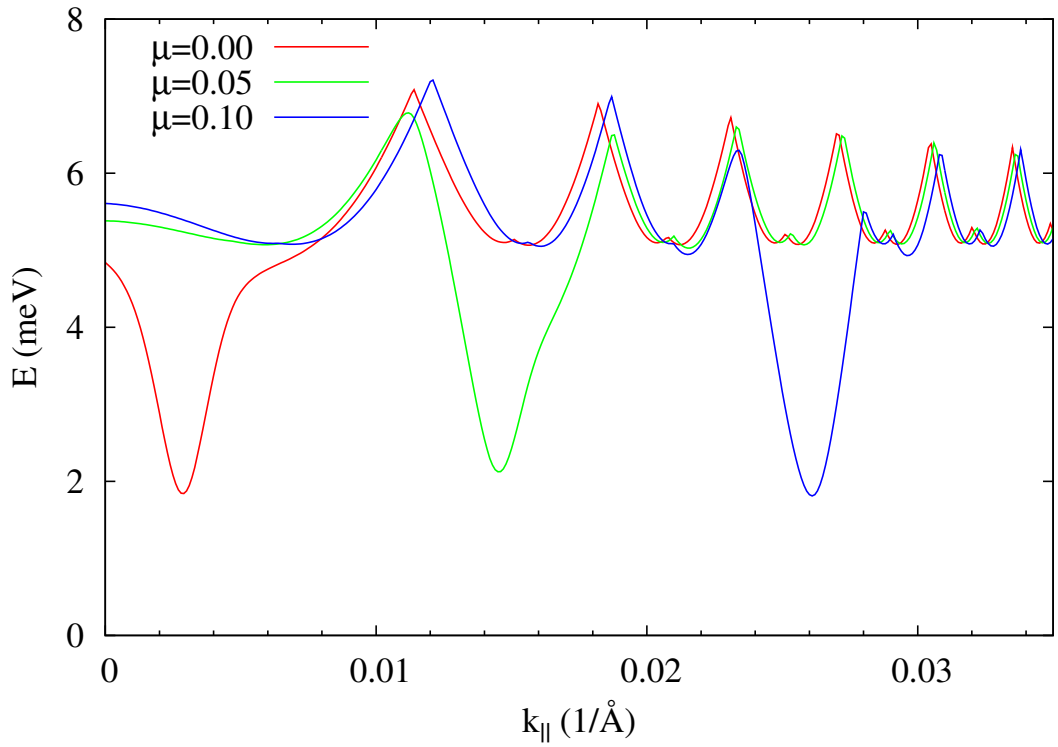

Figure 3.6: The dispersion of the lowest energy level for different μ (in eV). Other parameters are the same as in Fig. 3.5, $L = 160$nm and $\Delta_0 \sim 5.2$meV. Fu-Kane model well describes the lowest energy mode. As μ is increased, Δ_s and v_s stay roughly the same, while μ_s scales linearly with μ.

show no strong dependence on μ for this set of parameters. To make sure that the sub-gap mode is indeed localized near the interface, we plot in Fig. 3.7 the z dependence of the spectral function $N(k_\parallel, z, \omega)$. The spectral weight of the sub-gap mode is peaked near the interface and decays over a length scale $\sim \xi_0$ into the superconductor. This result clearly shows that for strongly coupled S-TI interfaces, the Fu-Kane model actually describe a rather "fat" interface mode. Note that the spectral weight on the TI side (not shown in the figure) is finite, but it is much smaller in magnitude and decays very fast inside TI. Finally, Fig. 3.8 shows the local density of states near the interface. The interface mode leads to finite density of states below the bulk gap, but the spectral weight is very small.

We have carried out similar analysis for superconductors with larger coherence length. Fig. 3.9 shows the evolution of the sub-gap mode with μ for $\Delta_0 = 2.4$meV. In this case, the

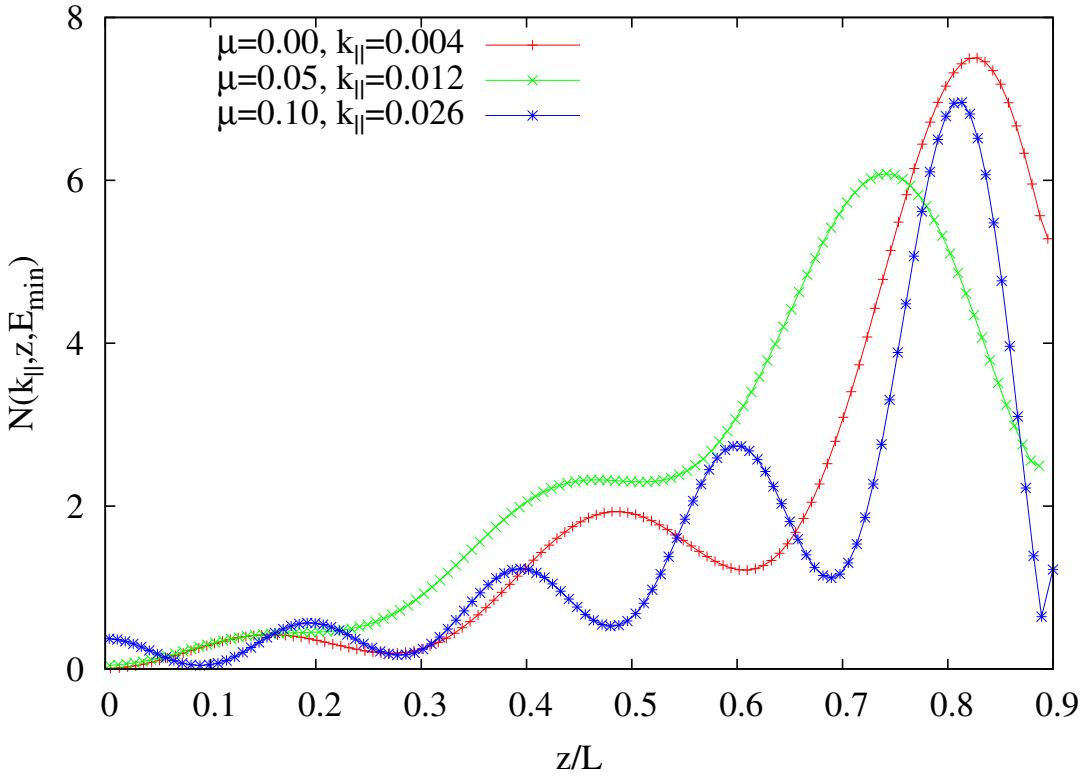

Figure 3.7: The spectral function $N(k_{\|}, z, \omega)$ of the lowest energy level, $\omega = E_{min}$, shown in Fig. 3.6. The interface is at $z = 0.9L$, L=160nm. The spectral function oscillates rapidly with z, so only its envelope is plotted.

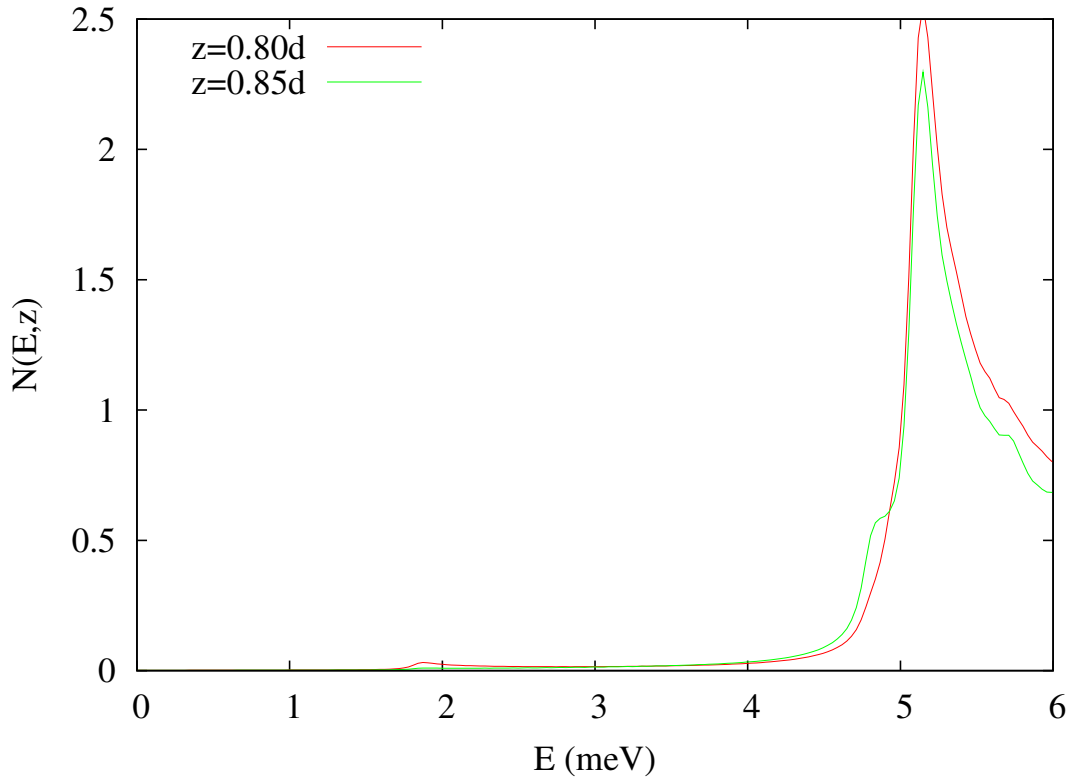

Figure 3.8: The local density of states $N(E, z)$ at $z = 0.8d$ and $z = 0.85d$ (the interface is at $z = 0.9d$). $\mu = 0$, $L = 160$nm, and $\Delta_0 \sim 5.2$meV. The subgap states are due to the interface mode. A level broadening $\sim 0.01\Delta_0$ is used.

values of (Δ_s, v_s, μ_s) all varies with μ. Superconductors with larger ξ_0 and smaller Δ_0 are thus more sensitive to changes in μ and other microscopic details near the interface. The exact values of the effective parameters in the Fu-Kane model in general depend on such microscopic details.

3.6 Triplet Pair Correlations

It is well known that in heterostructures of s-wave superconductors, pairing correlations in other orbital channels, e.g. p-wave correlations, will be induced by scattering at the interfaces [**?**, **?**]. For example, inversion/reflection symmetry ($z \leftrightarrow -z$) is lost in an S-TI proximity structure, and the appearance of p-wave correlations seems natural from partial wave analysis. Moreover, scattering by a topological insulator is spin-active. The spin-orbit

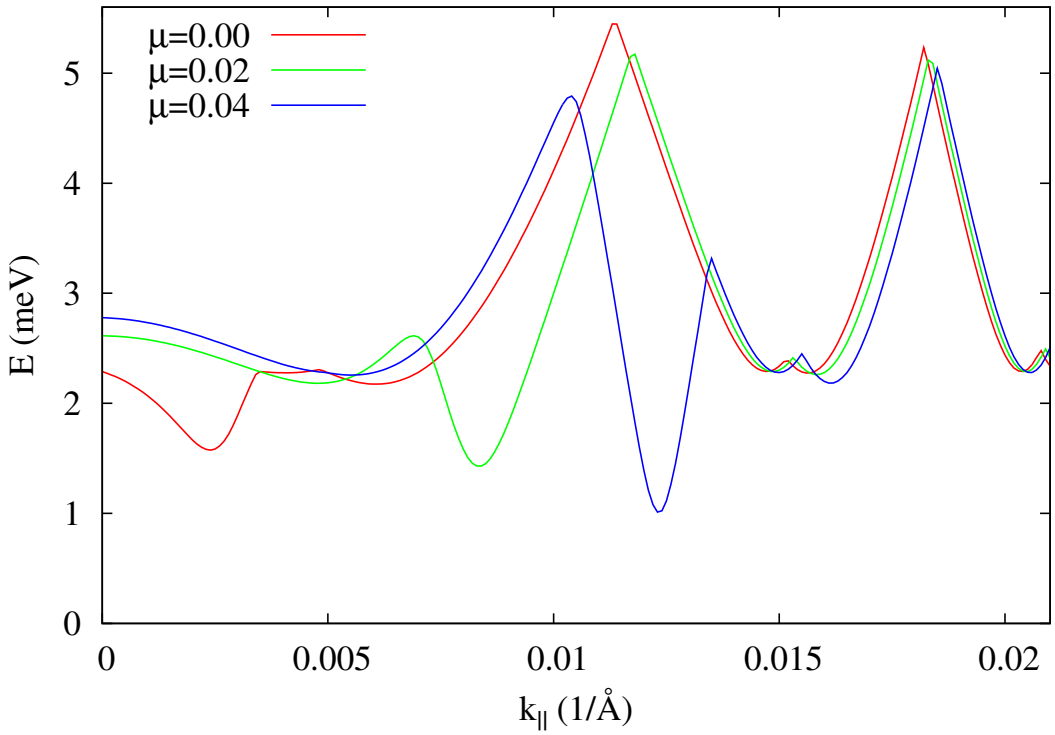

Figure 3.9: The lowest energy level of an S-TI structure with $L = 160$nm, $d = 0.9L$, $\Delta_0 = 2.4$meV. μ is the chemical potential of the TI and measured in eV.

coupling inside a TI acts like a momentum-dependent magnetic field to flip the electron spin and introduce different phase shifts for spin up and down electrons. The scattering matrix has been worked out by us previously [**?**]. Thus, a singlet s-wave Cooper pair can be converted into a pair of electrons in spin-triplet state at the S-TI interface. However, it is important to recall that by assumption attractive interaction only exists (or is appreciable) in the s-wave channel. There is no binding force to sustain a triplet Cooper pair or a triplet superconducting order parameter. Similar (but different) pairing correlations in superconductor-ferromagnet hybrid structures have been extensively studied [**?**]. The appearance of p-wave correlations in S-TI systems has been pointed out previously by Stanescu et al using a perturbative analysis [**?**].

We focus on the equal-time pair correlation functions defined in Eq. (3.30). By exploiting the symmetry of the BdG Hamiltonian, Eq. (3.19), we are able to find analytically the orbital structure of the triplet correlation functions. The unitary transformation Eq. (3.20) yields

$$\begin{aligned} u_{2\uparrow}(k_x, k_y) &= u_{2\uparrow}(k_\parallel, 0)e^{-i\varphi_k/2}, \\ u_{2\downarrow}(k_x, k_y) &= u_{2\downarrow}(k_\parallel, 0)e^{+i\varphi_k/2}, \\ v_{2\uparrow}(k_x, k_y) &= v_{2\uparrow}(k_\parallel, 0)e^{+i\varphi_k/2}, \\ v_{2\downarrow}(k_x, k_y) &= v_{2\downarrow}(k_\parallel, 0)e^{-i\varphi_k/2}. \end{aligned} \tag{3.34}$$

Using these relations, we find

$$F_{\uparrow\uparrow}(\mathbf{k}_\parallel, z) = F_{\uparrow\uparrow}(k_\parallel, z)e^{-i\varphi_k}, \tag{3.35}$$

$$F_{\downarrow\downarrow}(\mathbf{k}_\parallel, z) = F_{\downarrow\downarrow}(k_\parallel, z)e^{+i\varphi_k}. \tag{3.36}$$

Namely $F_{\uparrow\uparrow}$ ($F_{\downarrow\downarrow}$) has $p_x - ip_y$ ($p_x + ip_y$) orbital symmetry. Finally, the remaining triplet

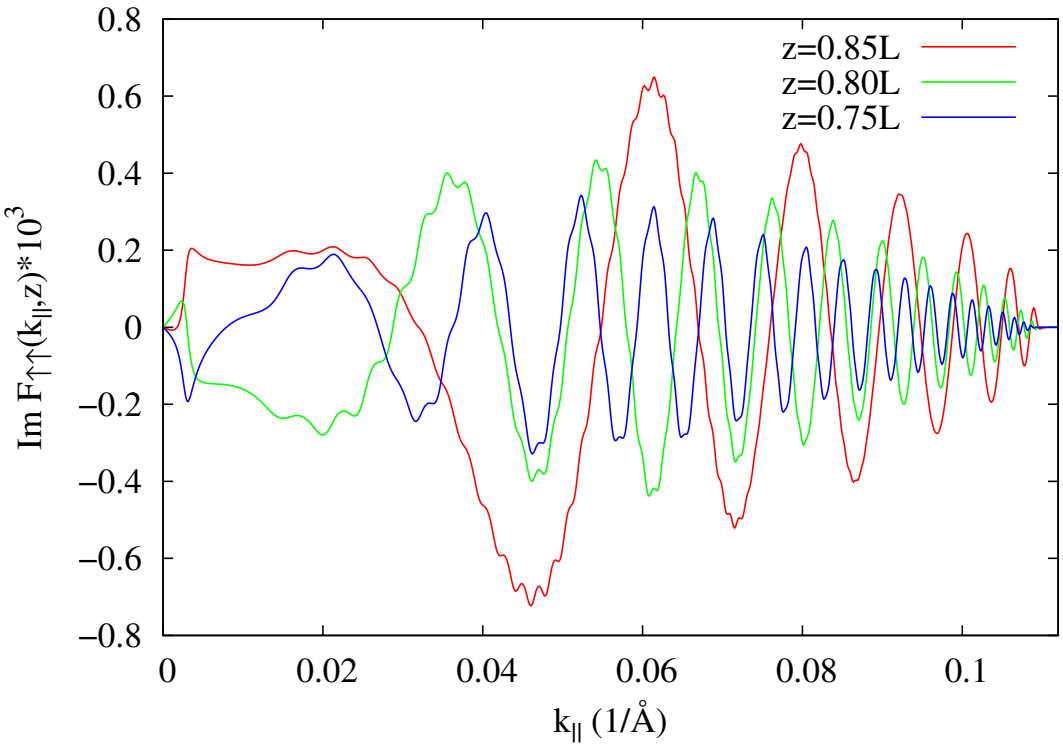

Figure 3.10: The imaginary part of triplet pair correlation function $F_{\uparrow\uparrow}(k_{\parallel}, z)$. The S-TI interface is at $d = 0.9L$. $\mu = 0$, $L = 160$nm, $\Delta_0 = 5.2$meV.

correlation function

$$\langle \psi_{2\uparrow}(\mathbf{k}_{\parallel}, z)\psi_{2\downarrow}(-\mathbf{k}_{\parallel}, z) + \psi_{2\downarrow}(\mathbf{k}_{\parallel}, z)\psi_{2\uparrow}(-\mathbf{k}_{\parallel}, z)\rangle \tag{3.37}$$

turns out to be zero. Note that the so-called odd-frequency paring correlations [**?**, **?**, **?**], which vanishes in the equal-time limit, are also interesting in S-TI structures, but we will not discuss their behaviors here.

We find that $F_{\uparrow\uparrow}(k_{\parallel}, z)$ is purely imaginary and identical to $F_{\downarrow\downarrow}(k_{\parallel}, z)$. The results for $\mu = 0$, $L = 160$nm, $d = 0.9L$, $\Delta_0 = 5.2$meV are plotted in Fig. 3.10. $F_{\uparrow\uparrow}$ vanishes at $k_{\parallel} = 0$ as well as for large $k_{\parallel}$, namely when $k_{\parallel} > \sqrt{(E_F + \omega_D + M)/B_2}$. This is consistent with lack of pairing in both limits. The behavior of $F_{\uparrow\uparrow}$ for small $k_{\parallel}$ is illustrated in Fig. 3.11 for $\mu = 0$, $L = 300$nm, $d = 0.95L$, $\Delta_0 = 0.6$meV. As comparison, we also plotted the singlet

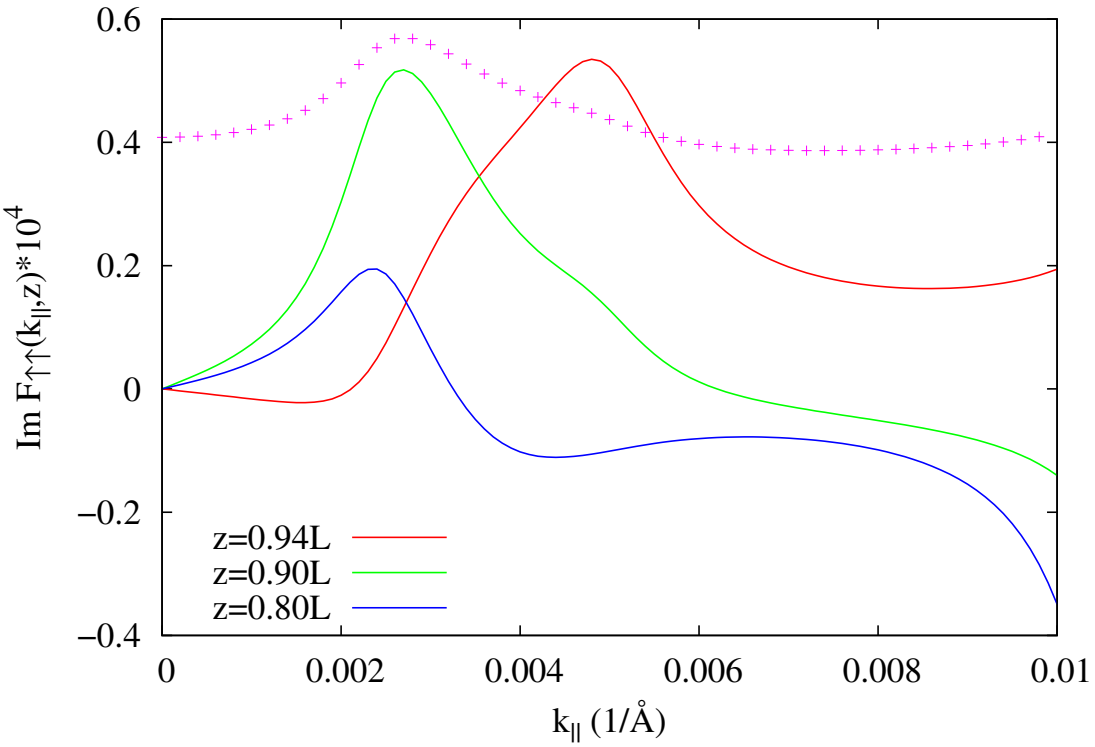

Figure 3.11: The imaginary part of $F_{\uparrow\uparrow}(k_\parallel, z)$. $\mu = 0$, $L = 300$nm, $d = 0.95L$, $\Delta_0 = 0.6$meV. As comparison, the data points show the singlet pair correlation function $F_{\uparrow\downarrow}(k_\parallel, z = 0.9L)/3$.

pair correlation function

$$F_{\uparrow\downarrow}(\mathbf{k}_\parallel, z) = \sum_n{}' u_{n,2\uparrow}(\mathbf{k}_\parallel, z) v^*_{n,2\downarrow}(-\mathbf{k}_\parallel, z) \tag{3.38}$$

which is s-wave and purely real.

3.7 Summary

In summary, we have investigated the proximity effect between an s-wave superconductor and a topological insulator using a microscopic continuum model. Strong coupling between the two materials renders the surface state of TI a less useful concept for this problem.

Our focus has been on the various modifications to superconductivity by the presence of TI. These include the suppression of the order parameter, the formation of interface modes below the bulk superconducting gap, and the induction of triplet pairing correlations. It is gratifying to see the Fu-Kane effective model emerges in the low energy sector albeit with a set of renormalized parameters. Our results are complementary to previous theoretical work on the proximity effect [**?**, **?**] and confirm the validity of the Fu-Kane model.

We made a few simplifying assumptions in our calculation. The superconductor is described by a two-band model with the valence band well below the Fermi level. Since only electrons near the Fermi surface are relevant for weak coupling superconductivity, we believe our main results are general. As idealizations, the chemical potential, the spin-orbit coupling, and the attractive interaction are assumed to be step functions with a sudden jump at the interface. More elaborate and realistic models can be considered within the framework of BdG equations. For example, one can add a tunneling barrier between S and TI, or include a Rashba-type spin-orbit coupling term (due to the gradient of chemical potential) at the interface. We will not pursuit these generalizations here. Finally, the approach outlined here can be straightforwardly applied to study non-Abelian superconductivity in other superconductor-semiconductor heterostructures where spin-orbit coupling also plays a significant role [**?**, **?**, **?**, **?**, **?**].

Chapter 4: Josephson Junction on TI Surface

Exotic excitations arise at the interface between a three-dimensional topological insulator (TI) and superconductors. For example, Majorana fermions with a linear dispersion, $E \sim k$, exist in a short π Josephson junction on the TI surface. We show that in these systems, the Andreev bound states spectrum becomes nearly flat at zero energy when the chemical potential is sufficiently away from the Dirac point. The flat dispersion is well approximated by $E \sim k^N$, where N scales with the chemical potential. Similar evolution from linear to flat dispersion also occurs for the subgap spectrum of a periodic superconducting proximity structure, such as a TI surface in contact with a stripe superconductor.

4.1 Introduction

Moving at "the speed of light", v_F, massless Dirac electrons on the surface of a three-dimensional Z_2 topological insulator (TI) can not be localized by scattering from nonmagnetic impurities [**?**, **?**], nor can they be easily confined by electrostatic potentials due to Klein tunneling [**?**]. Proximity coupling to ferromagnetic or superconducting order can however open up a gap in the spectrum, thus rendering excitations massive [**?**, **?**]. An intriguing possibility is to engineer new *massless* excitations by confining and coherently mixing Dirac electrons and holes using two or more superconductors with definite phase difference [**?**]. For example, Fu and Kane showed that a Josephson junction on the surface of a TI with a phase bias of π is a one-dimensional quantum wire for Majorana fermions, which can be further manipulated by using tri-junctions [**?**]. Signatures of Majorana fermions in such structures have been reported in recent experiments [**?**, **?**].

In this Letter, we demonstrate a drastically different regime for the same, albeit slightly

more general, Josephson structures considered by Fu and Kane. This regime features massless zero energy excitations that are almost dispersionless, i.e. with vanishing group velocity ($\partial E/\partial k \simeq 0$). We elucidate the scattering kinematics behind the nearly flat dispersion at zero energy using simple models, and verify the results with self-consistent calculations. We find it striking that in such simple structures, which are now available in experiments, the low energy excitation can be easily tuned all the way from $E \sim k$ to $E \sim k^N$, where N is large, by increasing the chemical potential. By extending such junctions into a class of *periodic* superconductor-TI proximity structures, we further show that these states become a flat band near zero energy.

4.2 Model

The Josephson junction is schematically shown in Fig. 4.1a). Two s-wave superconductors are patterned on the TI surface. Due to the proximity effect, the S-TI interface becomes a 2D superconductor (S). The S-TI-S junction can be well described by the following Bogoliubov-Dirac Hamiltonian introduced in Ref. [**?**],

$$\mathcal{H} = \hbar v_F(\sigma_x k_y + i\tau_z\sigma_y\partial_x) + \tau_z\mu(x) + \tau_y\sigma_y\Delta(x). \tag{4.1}$$

Here τ_i (σ_i) are the Pauli matrices in the particle-hole (spin) space. The system is translationally invariant in the y direction, and k_y is the momentum along y. In the TI region of length w, the superconducting order parameter $\Delta(x)$=0, while it is constant Δ deep into the superconductor. The chemical potential μ can be tuned by applying a gate voltage. In general, its value can differ in the TI and S region, but for simplicity, we assume it is uniform in all regions. Also, we will focus on the case of phase difference of π across the junction.

We first give a heuristic argument for the existence of two regimes. A Dirac electron in the TI region incident on S will be Andreev reflected into a hole if its energy is below the superconducting gap ($E < \Delta$). In the context of graphene [**?**, **?**], Beenakker pointed out

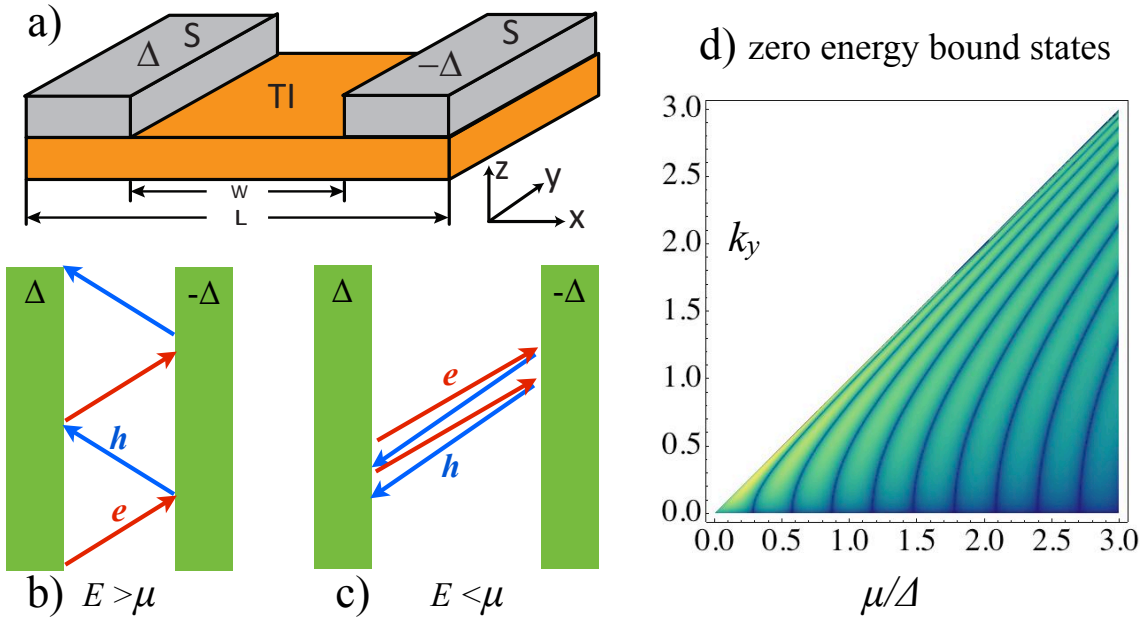

Figure 4.1: (color online) a) Schematic of a Josephson junction on the surface of a topological insulator (TI). The two superconducting leads (S) have a phase difference π. Δ is the superconducting gap, and w is the junction width (not to scale). b) Specular Andreev reflection in the regime $E > \mu$. c) Retro-reflection for $E < \mu$. d) Dark lines show the (k_y, μ) values for the zero energy Andreev bound states for $w = 10\hbar v_F/\Delta$ and $L \to \infty$. k_y is in unit of $\Delta/\hbar v_F$.

that in addition to the familiar Andreev retro-reflection where the reflected hole has a group velocity opposite to the incident electron when $E < \mu$, there is also the case of specular Andreev reflection where the reflected hole's group velocity is in the specular direction for $E > \mu$. Typical scattering trajectories in these two regimes are contrasted in Fig. 4.1b) and 4.1c). For $\mu = 0$ as considered in Ref. [**?**], the Majorana fermion excitation with linear dispersion is associated with the specular Andreev reflections in Fig. 4.1b). For large μ, as in the case of as grown Bi_2Se_3 crystals, one expects very different behaviors at low energies. For the $E < \mu$ case, it can be shown analytically that the phase of the retro-reflected hole is equal to the incident angle of an incoming electron at zero energy, $\theta = \arcsin(\hbar v_F k_y/\mu)$. This is unique to TIs because the wavefunction of a Dirac electron [or hole], $(1, \pm e^{i\theta}, 0, 0)$ $[(0, 0, 1, \pm e^{i\theta})]$, is determined by the angle θ, or k_y. The resultant hole incident on the opposite S with phase of π retro-reflects into an electron. This electron has exactly the same phase as it started with, thus forming an Andreev bound state.

The remaining key question is whether there will be any states at or near zero energy when μ is finite. We can answer the question by solving Eq. (4.1) for an idealized, step function profile of $\Delta(x)$,

$$\Delta(x) = \Delta[\theta(-x) - \theta(x - w)]. \tag{4.2}$$

The dark lines in Fig. 4.1d) shows the zero energy solution in the (μ, k_y) plane, with fixed Δ and the junction length $w = 10\hbar v_F/\Delta$. In general, there exist multiple zero energy bound states at discrete k_y values $\{k_y^i\}$ for finite μ. For increasing μ and w, these solutions become increasingly close-packed. This nontrivial result has important implications for experiments. The Majorana quantum wire is only ideal in the limit of $\mu, w \to 0$. As μ is tuned away from the Dirac point, the single zero energy state at $k = 0$ will be replaced by multiple zero energy solutions along the k_y axis, and eventually a nearly flat dispersion at zero energy.

To unambiguously establish this claim, we solve the differential equation $\mathcal{H}(x, k_y)\psi(x, k_y) = E\psi(x, k_y)$ numerically for a finite size system, $x \in [0, L]$ as shown in Fig. 4.1a), with open boundary conditions at $x = 0, L$ [**?**]. Here the quasiparticle wave function $\psi =$

$(u_\uparrow, u_\downarrow, v_\uparrow, v_\downarrow)^T$, with the label (x, k_y) omitted. To fully describe the proximity effect including the induced superconducting correlations in the TI region and the suppression of superconductivity near the TI-S boundary, we determine the order parameter profile $\Delta(x)$ self-consistently through the gap equation

$$\Delta(x) = g(x) \sum_{\epsilon_n < \omega_D} \int dk_y u_{n,\uparrow}(x, k_y) v^*_{n,\downarrow}(x, k_y). \tag{4.3}$$

Here n labels the eigenstates with energy ϵ_n, g is the effective attractive interaction, and ω_D is the Debye frequency. We assume g is zero in the TI region and constant inside S. We expand $\psi(x, k_y)$ and $\Delta(x)$ in Fourier series and convert the differential equation into an algebraic equation [**?**, **?**]. Starting with an initial guess of $\Delta(x)$ which features phase difference π, the iterative procedure is repeated until desired convergence is achieved. Note that the phase difference π is self-maintained throughout and not fixed by hand after every iteration. Then, the local spectral function,

$$A_\sigma(E, k_y, x) = \sum_n \delta(E - \epsilon_n) |u_{n\sigma}(x, k_y)|^2, \tag{4.4}$$

and the local density of states (LDOS),

$$N(E, x) = \int dk_y \sum_{n,\sigma} \delta(E - \epsilon_n) |u_{n\sigma}(x, k_y)|^2, \tag{4.5}$$

can be computed for $\sigma = \uparrow, \downarrow$. The calculation is checked to reproduce known results, e.g., the linearly dispersing Majorana spectrum at $\mu = 0$ predicted in Ref. [**?**].

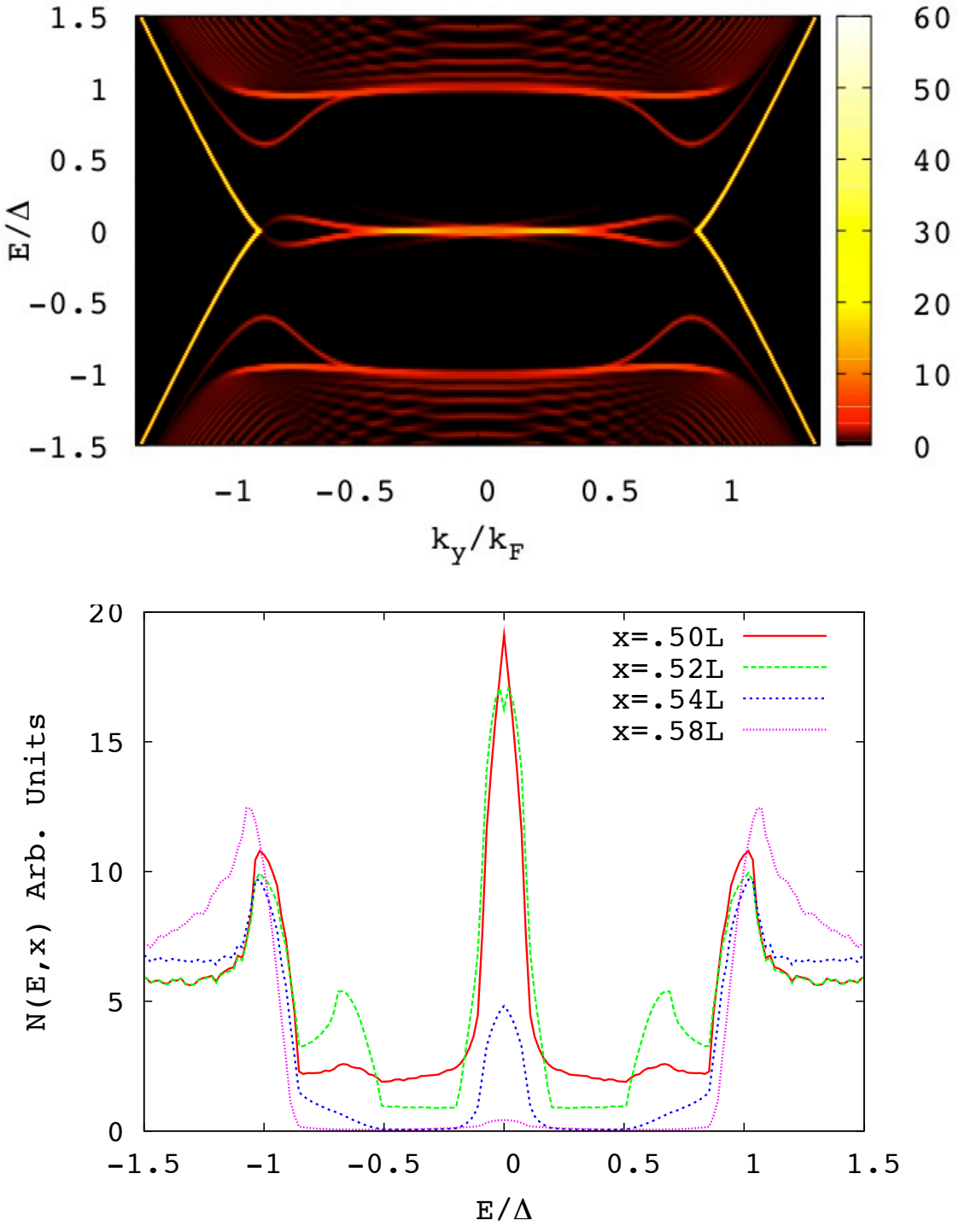

Figure 4.2: (color online) The local spectral function $A_\uparrow(E, k_y, x)$ (upper panel) and local density of states $N(E, x)$ (lower panel, red solid line) at the center of the junction, $x = 0.5L$. One sees "flat" Andreev bound states near zero energy for $-k_F < k_y < k_F$, and correspondingly a pronounced peak at zero energy in the LDOS in the lower panel. The lower panel also shows different LDOS away from the center, for x from $0.52L$ to $0.58L$.

4.3 Flat Bands in Spectrum

The upper panel of Fig. 4.2 shows the spectral function at the center of the junction, $A_\uparrow(E, k_y, x = 0.5L)$ ($A_\downarrow$ is the same for this value of x), with μ=20meV, Δ = 5.5meV, $w = 0.04L$, L = 2576nm, $\hbar v_F$=4.1 ÅeV, and the Fermi momentum $k_F = \mu/(\hbar v_F)$. In contrast to the $E \sim \hbar v_F k_y$ mode for $\mu = 0$, we see Andreev bound states (ABS) near zero energy within a wide region $-k_F < k_y < k_F$, where the slope $\hbar v_y = \partial E/\partial k_y$ approaches zero. The appearance of numerous crossings at exact zero energy for finite k_y also agrees with the model calculation above in Fig. 4.1d). Beyond this range, e.g. for $k_y > k_F$, the spectrum is reminiscent of the particle-hole folded dispersion of the helical metal, $E \sim \pm\hbar v_F(k_y - k_F)$.

As an approximate ansatz to describe the almost flat dispersion, we introduce the following phenomenological model for the ABS for large $\mu \gg \Delta$,

$$E/\Delta = c(k/k_F)^N, \tag{4.6}$$

where c is a constant and N is a large number. To fix N, we demand that the slope of the dispersion at energy $E \sim \Delta$ coincides with that of the bare dispersion, i.e., $\partial E/\partial k_y|_{E=\Delta} = \hbar v_F$. This gives an estimate of N,

$$N \simeq \mu/\Delta. \tag{4.7}$$

Note that we are only concerned with the ABS dispersion near zero energy and its continuation beyond k_F. For wider junctions, additional subgap ABS appear at finite energies, and they are not described by Eq. (4.6). Our ansatz is inspired by the mathematical theory of Dirac points with multiple topological charge N as found in multilayered system discussed in Ref. [**?**].

The flat dispersion implies a peak at zero energy in the local density of states. The lower panel of Fig. 4.2 shows the LDOS at the center of the junction, at the S-TI boundary, and slightly into the superconductor for the same junction parameters given above. While the zero energy peak becomes less pronounced when away from the junction center, it remains

clearly visible and persists even into the superconductor. Thus, the predicted flat ABS has a clear experimental signature in the tunneling conductance measurements.

The existence of two regimes including the flat Andreev bound states near zero energy is a general feature. We have carried out systematic, self-consistent simulations for the general case of an inhomogeneous chemical potential, e.g., $\mu(x) = \mu_{TI}$ within the TI region and $\mu(x) = \mu_S \neq \mu_{TI}$ inside the superconductors. The movie in the Supplementary Material shows the evolution of a typical spectrum for fixed μ_S with μ_{TI} gradually being increased from zero to μ_S [**?**]. We see the linear Majorana mode changing into the flat ABS.

4.4 Periodic π Junction

Having established the existence of nearly flat ABS around zero energy, now we systematically trace the evolution from the infinitesimal μ, linear dispersing (Majorana) regime to the large μ flat ABS regime. Also we would like to understand the details of ABS within its narrow "band width". To this end, we will consider a simple model which generalizes the π Josephson junction to periodic systems. Namely, in Eq. (4.1), the order parameter modulates sinusoidally in the x-direction with period $2a$ as schematically shown in the upper panel of Fig. 4.3,

$$\Delta(x) = \Delta \sin(\pi x/a). \tag{4.8}$$

The sign of the order parameter alternates. Thus the structure is effectively a periodic array of the π junctions discussed above in the limit $w \to 0$. One also recognizes that $\Delta(x)$ describes a stripe or Larkin-Ovchinnikov superconductor [**?**]. While such superconductors are hard to find, one may imagine bringing them in contact with a TI to realize the model consider here. Now the Hamiltonian $\mathcal{H}$ has discrete translational symmetry in the x-direction, $\mathcal{H}(x) = \mathcal{H}(x + 2a)$. We can apply the Bloch-Floquet theorem and introduce quasi-momentum k_x living in the Brillouin zone of $(-\pi/2a, \pi/2a)$. For the prescribed $\Delta(x)$, the energy spectrum $E(k_x, k_y)$ can be obtained by diagonalizing $\mathcal{H}$ in k-space. Note that the TI (non-superconducting) region is shrunk to a point, only the homogenous μ is left as

tuning parameter.

The lower panel of Fig. 4.3 shows the spectrum $E(k_x = 0, k_y)$ for $a = 24\hbar v_F/\Delta$, $\mu = 4\Delta$. These flat ABS at zero energy do not show significant variation with k_x. We have checked that the wave function of these zero energy states are localized at the domain wall boundaries of the order parameter field, i.e., at $x = ma$ (red curve in the upper panel of Fig. 4.3). For example, the wave function of the $k_y = 0, k_x = 0, E \approx 0$ mode can be fit well with periodic Gaussians $|u(x)| \propto \exp(-1.85(\pi x/\sqrt{2}a)^2)$. Since a is large in this case, these results agree well with the single junction result before. The dispersion, for example, can be fit well using the ansatz in Eq. (4.6). The vanishing band width is, of course, only valid on coarse scales. Closer inspection, by blowing up the spectrum near zero as illustrated in Fig. 4.4, reveals the busy life of the ABS with N_c crossings at zero energy, where N_c scales linearly with μ, in agreement with Fig. 4.1d). Remarkably, all these fine details are compressed within a small energy range.

Fig. 4.4 illustrates the evolution of the ABS at low energies for the periodic structure as μ is increased from zero. For small value of $\mu = 0.83\Delta$, the linear Majorana dispersion splits into two, each developing a curvature, as the zero energy crossings move to finite k_y values. Further increasing μ, these two crossings are stretched further outwards, while the dispesion within $k_y \in (-k_F, k_F)$ begin being bent and stretched to form the precursor of the flat band. At the same time, addition of new crossings introduces more twists. The number of crossing scales with $N_c \sim \mu/\Delta$. The spaghetti now becomes a rope, and looking from afar, it appears as a thin thread.

4.5 Summary

Flat bands are more novelties than the norm in condensed matter [**?**]. Recently, several authors have demonstrated that *surface* Andreev bound states with flat dispersion arise in certain topological superconductors, for example $Cu_xBi_2Se_3$ [**?**] and non-centrosymmetric

superconductors [?, ?]. Their existence can be traced back to the nontrivial topology associated with the gapped bulk, and thus are topologically protected. This mechanism giving rise to flat bands, via the bulk-boundary correspondence, differs from what is considered here. For example, in Ref. [?], a robust crossing at $k = 0$ is a crucial point in the argument, and the total number of zero energy crossings is guaranteed an odd number. In our case, states at $k_y = 0$ are gapped for finite size systems (or finite period $2a$). Despite these differences, the zero modes share the common trait that they are associated with the sign change of the order parameter when electrons are reflected at the surface or interface.

Several groups have successfully fabricated Josephson structures on Bi_2Se_3 of various length using a variety of superconducting materials including Al, Al/Ti, W, Nb, and Pb etc. [?, ?, ?, ?, ?]. Gate tunable supercurrent has been observed and argued to be due to the TI surface state [?]. Superconducting quantum interference devices based on such junctions have also been demonstrated [?, ?]. Thus the flat Andreev bound states at zero energy, and the zero bias conductance peak in the local density of states, predicted here should be experimentally accessible. Future work will explore control of these slowly dispersing Andreev levels working as qubits [?] when confinement in the y direction is also introduced. Our work also suggests the ac dynamics of the S-TI-S junctions will likely to be very complex featuring different regimes. The flat ABS at zero energy predicted for periodic junction arrays may potentially find technological applications. For example, a diverging density of states at the midgap may be used to generate microwave resonances.

We would like to thank Noah Bray-Ali, Liang Fu, and Takuya Kitagawa for helpful discussions.

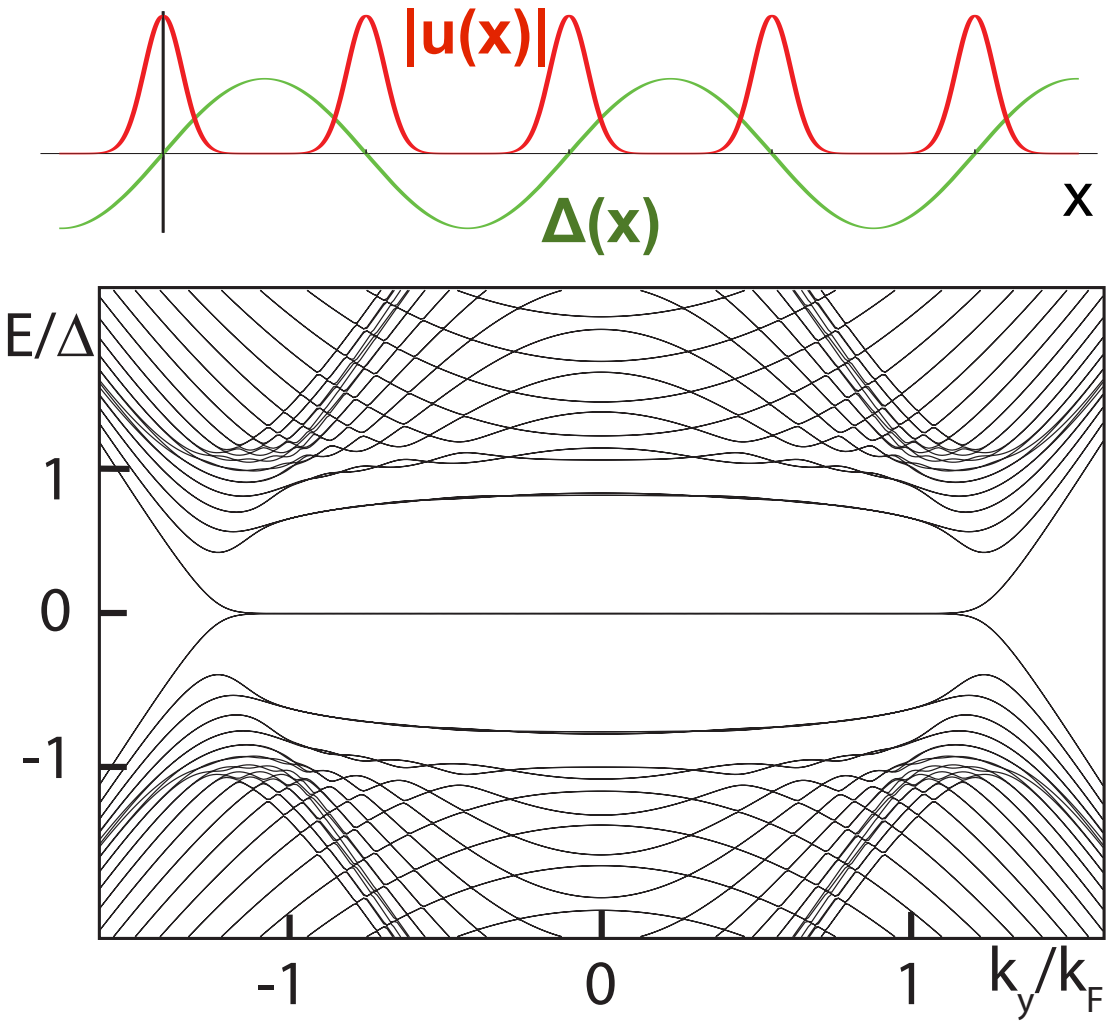

Figure 4.3: (color online) Upper panel: Schematic of the periodic proximity structure with $\Delta(x) = \Delta \sin(\pi x/a)$. The wave function $|u(x)|$ for the zero energy states are peaked at the domain wall boundaries, $x = ma$. Lower panel: Energy spectrum for $a = 24\hbar v_F/\Delta$ and $\mu = 4\Delta$ is flat at zero energy, which has fine structures upon closer inspection.

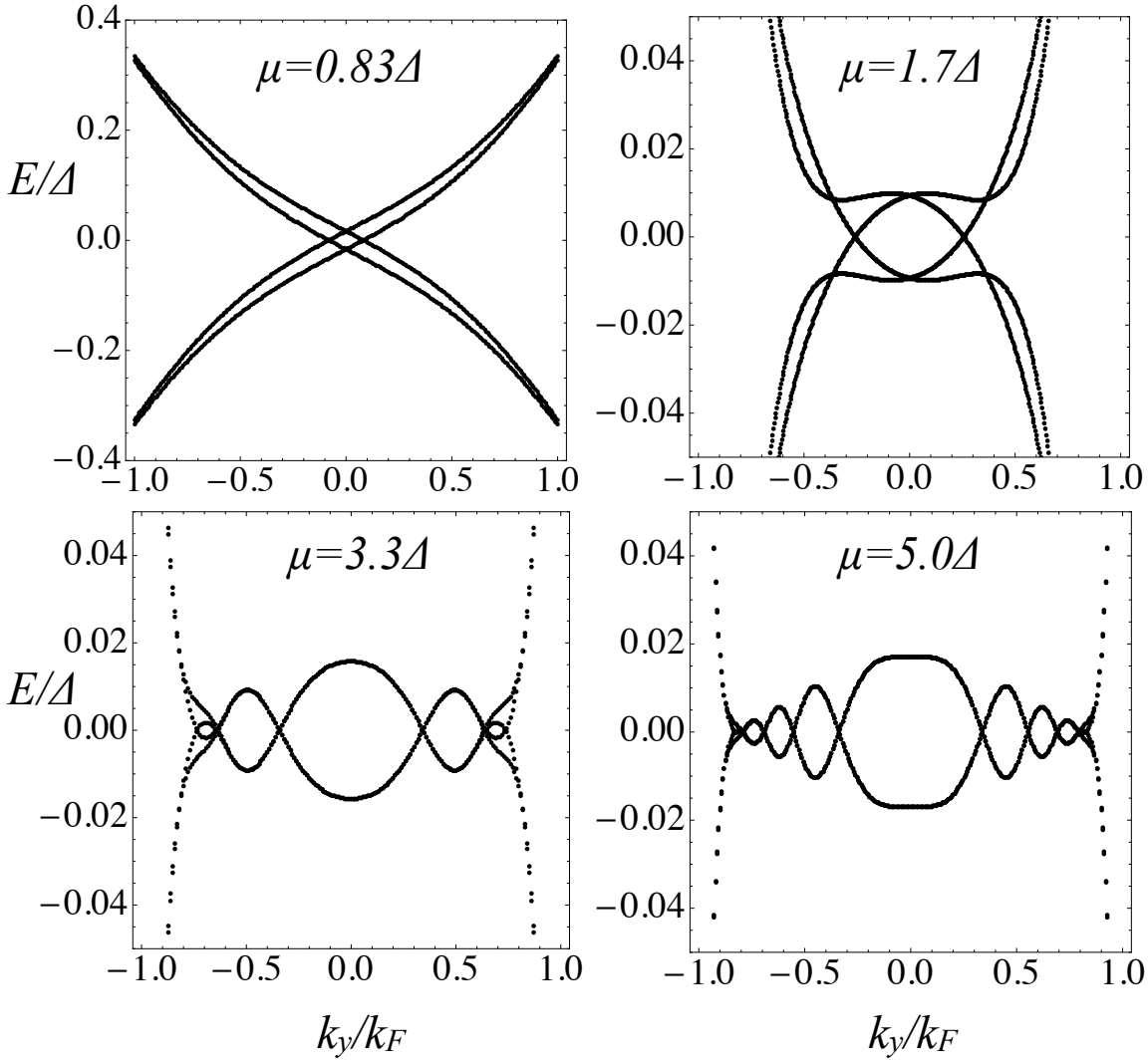

Figure 4.4: Fine structures in the energy spectrum of the periodic proximity structure with fixed $a = 12\hbar v_F/\Delta$ and increasing μ. The linearly dispersing Majorana spectrum at $\mu = 0$ splits and develops curvature to eventually become nearly flat within $(-k_F, k_F)$. The number of zero energy crossings increases with μ.

Bibliography

Bibliography